The Astrophysical Journal, 894:95 (25pp), 2020 May 10 https://doi.org/10.3847/1538-4357/ab8635

Cosmic-Ray Acceleration in Radio-jet Shear Flows: Scattering Inside and Outside the Jet

G. M. Webb[1], P. Mostafavi[2], S. Al-Nussirat[3], A. F. Barghouty[4], G. Li[1,5], J. A. le Roux[1,5], and G. P. Zank[1,5]
[1] Center for Space Plasma and Aeronomic Research, The University of Alabama in Huntsville, Huntsville, AL 35805, USA; gmw0002@uah.edu
[2] John Hopkins University, Applied Physics Lab., Laurel, MD 201723, USA
[3] Department of Physics and Astronomy, Louisiana State University, Baton Rouge, LA 70803, USA
[4] NASA HQ, Mail Code 7Z58, Quantum Science Program, HEOMD, Washington, DC 20546, USA
[5] Department of Space Science, The University of Alabama in Huntsville, Huntsville, AL 35899, USA
Received 2020 February 5; revised 2020 April 1; accepted 2020 April 1; published 2020 May 11

Abstract

A steady-state, analytical model of energetic particle acceleration in radio-jet shear flows due to cosmic-ray viscosity is explored, including particle scattering both into and out of the shear flow acceleration region. This involves solving a mixed Dirichlet–Von Neumann boundary value problem at the edge of the jet. The spectrum of the accelerated particles is harder than the free-escape case from the edge of the jet. The flow velocity $\boldsymbol{u} = u(r)\, \boldsymbol{e}_z$ is along the axis of jet (the z-axis). $\boldsymbol{u}$ is independent of distance z along the jet axis, and $u(r)$ is a monotonically decreasing function of cylindrical radius r from the jet axis. The scattering time $\tau(r, p) = \tau_0(p/p_0)^\alpha$ where p is the particle momentum in the fluid frame in the shear flow region $0 < r < r_2$, and $\tau(r, p) = \tau_0(p/p_0)^\alpha(r/r_2)^s$ outside the jet ($r > r_2$). Green's functions are obtained for monoenergetic injection of particles with momentum $p = p_0$ at radius $r = r_1$ ($0 < r_1 < r_2$). The Green's function and Green's formula are used to determine solutions for a general spectrum of particles at $r = \infty$. Solutions are obtained corresponding to a monoenergetic spectrum at infinity. We discuss the implications of these results for the acceleration of ultra-high-energy cosmic-rays in active galactic nucleus jet sources. Leaky box models of particle acceleration in shear flows, including synchrotron losses and particle escape, are used to describe the momentum spectrum of accelerated particles. The use of the relativistic telegrapher transport equation model is discussed.

Unified Astronomy Thesaurus concepts: Cosmic rays (329); Ultra-high-energy cosmic radiation (1733); Radio jets (1347); Relativistic jets (1390)

1. Introduction

The origin and acceleration of high-energy cosmic-rays is an ongoing quest in cosmic-ray astrophysics (e.g., Axford 1981, 1994; Hillas 1984; Biermann & Strittmatter 1987; Protheroe & Szabo 1992; Rachen & Biermann 1993; Rachen et al. 1993; Dermer 2007; Blandford et al. 2014).

The acceleration of cosmic-rays to ultra-high energies by cosmic-ray viscosity in astrophysical shear flows has been investigated by a number of authors (e.g., Berezhko 1981, 1982, 1983; Berezhko & Krymsky 1981; Earl et al. 1988; Jokipii et al. 1989; Webb 1989, 1990; Jokipii & Morfill 1990; Ostrowski 1990, 1998, 2002; Webb et al. 1994, 2018a, 2019; Rieger & Mannheim 2002; Stawarz & Ostrowski 2002; Rieger & Duffy 2004, 2005a, 2005b, 2006, 2016, 2019; Ohira 2013; Liu 2015; Liu et al. 2017; Kimura et al. 2018; Rieger 2019).

Other particle acceleration mechanisms in astrophysical fluid flows include second-order Fermi acceleration (e.g., Achterberg 1979; Bicknell & Melrose 1982; Schlickeiser 2002) and first-order Fermi acceleration at shocks (e.g., Axford et al. 1977; Krymsky 1977; Bell 1978a, 1978b; Blandford & Ostriker 1978; Drury 1983; Malkov & Drury 2001). Some models of particle acceleration by shock waves also include the effect of second-order Fermi acceleration (e.g., Webb 1983; Krülls 1992; Schlickeiser 2002). First-order Fermi acceleration at relativistic shocks using the pitch angle focusing transport equation was developed by Kirk & Schneider (1987a, 1987b). Particle acceleration at relativistic shocks were reviewed by Kirk & Duffy (1999), Achterberg et al. (2001), and Pelletier et al. (2017). Acceleration mechanisms for energetic particles in reconnecting magnetic flux ropes and magnetic fields (Drake et al. 2013; Zank et al. 2014, 2015; Guo et al. 2015; le Roux et al. 2015, 2016, 2019; Li et al. 2017) have been developed to explain spacecraft observations of particles in the heliosphere (e.g., Khabarova et al. 2017).

Lemoine (2019) has developed a statistical approach to generalized Fermi acceleration in which the affine connection coefficients describing non-inertial and gravitational forces are included in the Lorentz force equation (see also Webb 1985, 1989; Achterberg & Norman 2018a, 2018b) and has applied the formalism to determine the systematic acceleration rate and the second-order moments describing the particle acceleration, with application to a variety of scenarios (e.g., first-order Fermi acceleration at both nonrelativistic and relativistic shocks; shear acceleration, centrifugal acceleration in rotating flows, unipolar induction, and to particle energization in black hole applications).

Matthews et al. (2019) and Bell et al. (2019) argue that the acceleration of ultra-high-energy cosmic-rays (UHECR) can be produced by diffusive shock acceleration (DSA) by shocks in the back-flowing material of radio-jet galaxies lobes (e.g., in Faranoff–Riley type II jets). Araudo et al. (2016, 2018) argue that observations of radio-jet hotspots suggest that jet termination shocks are not likely to accelerate cosmic-rays to Eev energies.

In this paper, we obtain generalized versions of the solutions of the relativistic diffusive transport equation for particle acceleration in radio-jet shear flows obtained by Webb et al. (2018a, 2019). In these solutions, the flow velocity profile has the form $\boldsymbol{u} = u(r)\, \boldsymbol{e}_z$ along the axis of the jet (the z-axis) in which $u(r)$ is a monotonically decreasing function of cylindrical radius r about the z-axis. The solutions of Webb et al. (2018a, 2019) assumed that the particles were accelerated by the shear flow in the region $0 < r < r_2$ and free escaped through the boundary at $r = r_2$, or alternatively entered the inner region through $r = r_2$. In this paper, the Green's function solution and other solutions of the diffusive transport equation obtained by Webb et al. (2018a, 2019) are generalized to take into account particle scattering in the region $r > r_2$. This is achieved by solving a Dirichlet–Von Neumann boundary value problem at the edge of the jet at $r = r_2$, which takes into account a finite scattering time $\tau(r, p)$ in the region $r > r_2$. The solutions are obtained for the case $\tau = \tau_0(p/p_0)^\alpha$ in the region $0 < r < r_2$ and $\tau = \tau_0(p/p_0)^\alpha (r/r_2)^s$ in the region $r > r_2$ where s is a positive constant. It turns out that the family of possible solutions can be parameterized by a single parameter ϵ in which $\epsilon = 0$ recovers the solutions of Webb et al. (2019) corresponding to a free-escape boundary at $r = r_2$. For $\epsilon \gg 1$, the particles exiting the inner region have a high probability of reentry into $0 < r < r_2$ leading to enhanced particle acceleration to higher energies compared to the free-escape case with $\epsilon = 0$.

The parameter $\epsilon = k/s$, where $s = \partial \ln(\tau)/\partial \ln(r)$ in the outer region $r > r_2$, and k is a positive constant proportional to the velocity shear gradient, i.e., $k = g(\beta)\partial\beta/\partial \ln(r)$ where $g(\beta)$ is a complicated, monotone function of β defined in the region $0 < r < r_2$, and $\beta = u/c$ where c is the speed of light. Thus, ϵ measures the ratio of the velocity shear gradient modified by the factor $g(\beta)$ in $0 < r < r_2$ divided by the the parameter s, which depends on the diffusion coefficient gradient in $r > r_2$. The form of the flow velocity profile $\beta = \beta(r)$ has a very specific form, chosen to be a monotonic function of r that allows the transport equation to be written in a separable form (compare with a similar transformation choice used by Drury et al. 1982 in the analysis of particle momentum spectra for a smooth cosmic-ray modified shock).

Section 2 introduces the basic relativistic transport equations for cosmic-rays in relativistic flows obtained by Webb (1989). The mixed Dirichlet–Von Neumann boundary conditions involve both f_0 and $\partial f_0/\partial r$ at the boundary $r = r_2$. The boundary conditions are derived by matching the solution forms on both sides of the boundary.

Section 3 derives the Green's function solution in the inner region $0 < r < r_2$ satisfying the Dirichlet–Von Neumann boundary condition by using a Fourier–Bessel solution ansatz similar to that used in Webb et al. (2019) to derive the free-escape boundary Green's function.

In Section 4, Green's formula for the transport equation is used in conjunction with the Green's function from Section 3, satisfying the mixed Dirichlet–Von Neumann boundary condition at $r = r_2$ to obtain solutions in which the distribution function spectrum is specified as $r \to \infty$ as $f_0(\infty, p)$. The Green's formula gives the solution of the boundary value problem in the region $0 < r < r_2$, and the solution form in $r > r_2$ is readily obtained once $f_0(r_2, p)$ is calculated. The specific case of a monoenergetic spectrum as $r \to \infty$, i.e., $f_0(\infty, p) = N_g \delta(p - p_0)/(4\pi p_0^2)$ is given in closed form as a Fourier–Bessel series.

Section 5 gives estimates of the shear acceleration process and its modification by particle losses and escape from the acceleration region. Astrophysical applications are discussed. Section 5.1 provides a discussion of the shear acceleration transport equation, and it is generalized to include telegrapher equation terms that take into account the cosmic-ray inertia. Section 5.2 calculates the mean time $\langle t(p; p_0)\rangle$ for particles to be accelerated (decelerated) from $p = p_0$ to momentum p at time t, based on the time-dependent Green's function for particle acceleration in a shear flow obtained by Berezhko (1982; see also Rieger & Duffy 2006). It is shown that $\langle t(p; p_0)\rangle$ for the Green's function in Berezhko (1982), implies that particles can be accelerated from $p = p_0$ up to an infinite momentum in a finite time. This unphysical result is possibly due to neglecting particle escape from the acceleration region or due to the neglect of the cosmic-ray inertia, which is present in the generalized diffusive, telegrapher transport equation alluded to in Webb et al. (2018a, 2019). The telegrapher transport equation characteristics provide a formula that predicts a finite particle momentum at a finite time t. Section 5.3 studies leaky box models for particle acceleration, including synchrotron losses and particle escape and its relation to the solutions in Sections 3 and 4. Section 5.4 gives estimates of timescales and of the steady-state asymptotic spectral index μ_∞. Details of the calculations are relegated to the appendices.

Section 6 concludes with a summary and conclusions.

2. Model and Equations

The basic model for particle acceleration in a relativistic jet shear flow is essentially the same as that used by Webb et al. (2018a, 2019). The particle scattering is assumed sufficiently strong that an isotropic scattering and diffusion model may be used, and it uses the diffusive transport equation for cosmic-rays in relativistic flows obtained by Webb (1989; see also Achterberg & Norman 2018a, 2018b for similar formulations). The scattering wave frame for the particles is taken as coincident with the background plasma flow frame (i.e., the co-moving fluid frame). We neglect the effects of second-order Fermi acceleration. The transport equation for the isotropic distribution function of the particles $f_0(x^\alpha, p)$ ($x^\alpha = (ct, x, y, z)$ is the spacetime position four-vector of the particle) has the form (Webb 1989):

$$\begin{aligned}
&\nabla_\alpha\left[cu^\alpha f_0 - \kappa(g^{\alpha\beta} + u^\alpha u^\beta)\right.\\
&\quad\left.\times\left(\frac{\partial f_0}{\partial x^\beta} - \dot{u}_\beta \frac{(p^0)^2}{p}\frac{\partial f_0}{\partial p}\right)\right]\\
&\quad + \frac{1}{p^2}\frac{\partial}{\partial p}\left[-\frac{p^3}{3}cu^\beta_{;\beta} f_0 + p^3\left(\frac{p^0}{p}\right)^2 \kappa \dot{u}^\beta\right.\\
&\quad \times\left(\frac{\partial f_0}{\partial x^\beta} - \dot{u}_\beta \frac{(p^0)^2}{p}\frac{\partial f_0}{\partial p}\right)\\
&\quad \left. - \Gamma\tau p^4 \frac{\partial f^0}{\partial p}\right] = Q. \qquad (1)
\end{aligned}$$

In the case of strong scattering ($\omega\tau \ll 1$ where $\omega = qB/m$ is the gyro-frequency and τ is the scattering time), the viscous momentum coefficient Γ is given by

$$\Gamma = \frac{c^2}{30}\sigma_{\alpha\beta}\sigma^{\alpha\beta}, \qquad (2)$$

where $\sigma_{\alpha\beta}$ is the relativistic shear tensor of the fluid (see, e.g., Webb et al. 2019 for more detail).

$$\sigma_{\alpha\beta} = u_{\alpha;\beta} + u_{\beta;\alpha} + u_\beta \dot{u}_\alpha + u_\alpha \dot{u}_\beta - \frac{2}{3}u^\gamma_{;\gamma}(g_{\alpha\beta} + u_\alpha u_\beta) \qquad (3)$$

is the shear tensor of the background flow (a more conventional form of the shear tensor is one-half of the tensor in (3)). More general forms of the transport equation for both weak and strong scattering are described in Webb (1989).

We use the model of Webb et al. (2018a, 2019), in which the jet fluid velocity is assumed to be of the form

$$\boldsymbol{u} = u(r)\boldsymbol{e}_z, \tag{4}$$

where $u(r)$ is a monotonically decreasing function of r. For the fluid velocity profile (4), the acceleration vector of the fluid $\dot{u}_\alpha = 0$, and the divergence of the fluid velocity four-vector $u^\beta_{;\beta} \equiv \nabla_\beta u^\beta = 0$. The net result is a model in which the particles are accelerated solely due to cosmic-ray viscosity and shear of the background flow.

The scattering time $\tau(r, p)$ for particles with momentum p as measured in the fluid frame has the form $\tau = \tau_0(p/p_0)^\alpha$ in the shear flow region $0 < r < r_2$ about the jet axis, and $\tau = \tau_0(p/p_0)^\alpha(r/r_2)^s$ in the region $r > r_2$.

From Webb et al. (2018a, 2019), the viscous shear acceleration coefficient for the model is given by

$$\Gamma = \frac{c^2}{15}\gamma^4\left(\frac{d\beta}{dr}\right)^2 = \frac{\gamma^4}{15}\left(\frac{du}{dr}\right)^2. \tag{5}$$

For steady-state solutions of Equation (1), we assume there is no z-dependence to the solution. In this case, Equation (1) reduces to the form

$$-\frac{1}{r}\frac{\partial}{\partial r}\left(\kappa r\frac{\partial f_0}{\partial r}\right) - \frac{c^2}{15}\gamma^4\left(\frac{d\beta}{dr}\right)^2\frac{1}{p^2}\frac{\partial}{\partial p}\left(p^4\tau\frac{\partial f_0}{\partial p}\right) = Q \tag{6}$$

where $\beta = u/c$, and the source term Q has the form

$$Q = \frac{N_0}{8\pi^2 p_0^2 r_1}\delta(p - p_0)\delta(r - r_1), \tag{7}$$

in the case of monoenergetic injection of particles from $r = r_1$ with $p = p_0$.

2.1. Mixed Boundary Conditions

In this subsection, we discuss a modified boundary condition to apply to the particle momentum spectrum $f_0(r, p)$ and $\partial f_0/\partial r$ at the edge of the jet at a cylindrical radius $r = r_2$. The boundary condition used in Webb et al. (2018a, 2019) was that $f_0(r_2, p)$ is specified at the edge of the jet at $r = r_2$. This boundary condition does not explicitly address the particle transport in the region $r > r_2$. It could be interpreted as the solution of the transport Equation (6), with $\kappa \to \infty$ in $r > r_2$.

If one assumes there is no particle acceleration in $r > r_2$, but the diffusion coefficient is given in $r > r_2$, then the particle transport Equation (6) in $r > r_2$ reduces to

$$-\frac{1}{r}\frac{\partial}{\partial r}\left(r\kappa\frac{\partial f_0}{\partial r}\right) = 0, \tag{8}$$

where, for simplicity, we assume that $Q(r, p) = 0$ in $r > r_2$. The solution of Equation (8) in $r > r_2$ has the form

$$f_0(r, p) = C(p)\int_{r_2}^{r}\frac{dr'}{r'\kappa(r', p)} + D(p), \tag{9}$$

where $C(p)$ and $D(p)$ are "integration constants", and we assume that the integral in Equation (9) is finite. Note that

$$\kappa r\frac{\partial f_0}{\partial r} = C(p) \tag{10}$$

is a first integral of Equation (8). From Equation (10), it follows that

$$C(p) = r_2\kappa(r_2, p)\frac{\partial f_0(r_2, p)}{\partial r} \tag{11}$$

may be identified as the diffusive particle flux at $r = r_2$.

Letting $r \to \infty$ in solution (9), we obtain

$$D(p) = f_0(\infty, p) - r_2\kappa(r_2, p)\frac{\partial f_0(r_2, p)}{\partial r}\left(\int_{r_2}^{\infty}\frac{dr'}{r'\kappa(r', p)}\right), \tag{12}$$

for the unknown function $D(p)$. Using Equations (11) and (12) for $C(p)$ and $D(p)$, we obtain the solution for $f_0(r, p)$ in $r \geqslant r_2$ as

$$f_0(r, p) = f_0(\infty, p) - r_2\kappa(r_2, p)\frac{\partial f_0(r_2, p)}{\partial r}\left(\int_{r}^{\infty}\frac{dr'}{r'\kappa(r', p)}\right). \tag{13}$$

Setting $r = r_2$ in Equation (13) gives the boundary condition at $r = r_2$ as

$$f_0(r_2, p) + r_2\kappa(r_2, p)\frac{\partial f_0(r_2, p)}{\partial r}\left(\int_{r_2}^{\infty}\frac{dr'}{r'\kappa(r', p)}\right) = f_0(\infty, p). \tag{14}$$

The boundary condition of Equation (14) is central to the present paper. It is a mixed Dirichlet–Von Neumann boundary condition on the solution for $f_0(r, p)$ describing particle acceleration by shear in the jet. In Webb et al. (2018a, 2019), it was assumed that $\kappa \to \infty$ in the region $r > r_2$. In that case, the boundary condition becomes a Dirichlet boundary condition in which f_0 is specified on the boundary at $r = r_2$. In the more general case, when particle scattering outside the jet in the region $r > r_2$ is taken into account, then it is essential to also take into account the spatial gradient of f_0 at $r = r_2$ via the $\partial f_0/\partial r$ term at $r = r_2$. It was speculated by Webb et al. (2019) that the modified boundary condition of Equation (14) would give rise to harder accelerated particle spectra at momenta $p \gg p_0$ because particles that had exited the system at $r = r_2$ could now reenter the region and become further accelerated by the shear flow in $r < r_2$.

In order to get a better feel for the implications of the boundary condition of Equation (14), consider the case where

$$\kappa(r, p) = \frac{c^2\tau_0}{3}\left(\frac{p}{p_0}\right)^\alpha\left(\frac{r}{r_2}\right)^s, \quad (s > 0). \tag{15}$$

Using Equation (15) in Equation (13), we obtain

$$f_0(r, p) = f_0(\infty, p) - \frac{r_2}{s}\frac{\partial f_0(r_2, p)}{\partial r}\left(\frac{r_2}{r}\right)^s, \tag{16}$$

for f_0 in $r > r_2$.

The boundary condition of Equation (14) then becomes

$$f_0(r_2, p) + \frac{r_2}{s}\frac{\partial f_0(r_2, p)}{\partial r} = f_0(\infty, p). \qquad (17)$$

The boundary condition of Equation (17) is a mixed Dirichlet–Von Neumann boundary condition. For $s \gg 1$, Equation (17) is approximately the Dirichlet boundary condition

$$f_0(r_2, p) \approx f_0(\infty, p), \qquad (18)$$

which is the free-escape boundary condition used by Webb et al. (2018a, 2019). In the opposite limit ($s \to 0$), the boundary condition of Equation (17) appears to reduce to an approximate Neumann boundary condition,

$$\frac{r_2}{s}\frac{\partial f_0(r_2, p)}{\partial r} \approx f_0(\infty, p). \qquad (19)$$

Intuitively, we expect that the boundary condition of Equations (14) or (17) will lead to harder particle spectra, because particles crossing $r = r_2$ into the region $r > r_2$ may now return back into the region $r < r_2$ to be further accelerated by the shear flow inside $r = r_2$.

It is clear that one could also include a source term $Q(r, p)$ on the right-hand side of Equation (6) in the region $0 < r < r_2$. Similarly, one could include sources of particles in the region $r > r_2$. A slightly more general version of the boundary condition (17) for the case of a separable diffusion coefficient $\kappa(r, p) = \kappa_0(p)\kappa_1(r)$ is given in Appendix B.

2.2. Boundary Conditions as r → 0

The steady-state Green's function of Equation (6) describes the particle transport and acceleration in the region $0 < r < r_2$, where particles are injected monoenergetically into the flow with momentum $p = p_0$ at radius $r = r_1$ $(0 < r_1 < r_2)$. It is assumed that there are no sources of particles on the axis of the jet at $r = 0$. The boundary condition on the solution for $f_0(r, p)$ as $r \to 0$ (see Paper I) is

$$rS_d = r\left(-4\pi p^2 \kappa \frac{\partial f_0}{\partial r}\right) \quad \to \quad 0 \quad \text{as} \quad r \quad \to \quad 0. \qquad (20)$$

The source term of Equation (7) describes the steady injection of particles with momentum $p = p_0$ at radius $r = r_1$. The model can be applied to the case of a "naked" jet in which there is no back-flowing cocoon ($u(r) > 0$), or with a back-flowing cocoon with $u > 0$ near $r = 0$ and monotonically decreasing with $u < 0$ at large r (i.e., the case of a back-flowing cocoon; e.g., Webb et al. 2018a).

2.3. Transport Equation (6) Reduction for 0 < r < r₂

To obtain analytical solutions of the transport Equation (6), we use the new independent variables

$$\xi(r) = \frac{1}{2}\ln\left(\frac{1+\beta}{1-\beta}\right) = \tanh^{-1}(\beta), \qquad T = \ln\left(\frac{p}{p_0}\right), \qquad (21)$$

and assume a scattering mean free time $\tau(r, p)$ of the form

$$\tau = \tau_0\ (p/p_0)^\alpha g(\xi)/[r(d\xi/dr)], \qquad (22)$$

where $g(\xi)$ is an arbitrary function of ξ, and α is constant determining the momentum dependence of mean scattering time τ. Note that ξ is a monotonically increasing function of β.

With these choices, the transport Equation (6) with the source term of Equation (7) reduces to

$$\frac{1}{g(\xi)}\frac{\partial}{\partial \xi}\left(g(\xi)\frac{\partial f_0}{\partial \xi}\right) + \frac{1}{5}\left(\frac{\partial^2 f_0}{\partial T^2} + (3+\alpha)\frac{\partial f_0}{\partial T}\right) = \frac{3N_0\delta(T)\delta(\xi - \xi_1)}{8\pi^2 p_0^3 c^2 \tau_0 g(\xi_1)}. \qquad (23)$$

Here, $\xi_1 \equiv \xi(r_1)$ is the value of ξ at $r = r_1$ (see Webb et al. 2018a).

At this point, we choose an appropriate functional form for $g(\xi)$, which determines the scattering time $\tau(r, p)$ in Equation (22). As in Webb et al. (2018a), we consider only ultra-relativistic particles for which the particle speed $v \sim c$ in the fluid frame, where c is the speed of light, and the particle diffusion coefficient $\kappa \sim c^2\tau/3$. We choose

$$g(\xi) = k(\xi - \xi_0). \qquad (24)$$

In the case of Equation (24), we choose ξ so that

$$\frac{g(\xi)}{r d\xi/dr} = \frac{k(\xi - \xi_0)}{r d\xi/dr} = 1, \qquad (25)$$

where k is a positive constant. For these choices, we obtain

$$\tau = \tau_0\left(\frac{p}{p_0}\right)^\alpha. \qquad (26)$$

Integrating Equation (25) leads to the class of shear flows, for which

$$\xi = \xi_0 - (\xi_0 - \xi_2)\left(\frac{r}{r_2}\right)^k, \qquad \beta(r) = \tanh(\xi). \qquad (27)$$

If we choose $k > 1$, then $d\xi/dr \to 0$ as $r \to 0$, but if $0 < k < 1$, then $d\xi/dr \to \infty$ as $r \to 0$. For the case $k = 1$, $d\xi/dr \to -\xi_{02}/r_2$ as $r \to 0$ where $\xi_{02} = \xi_0 - \xi_2$. We choose the cases $k \geqslant 1$, which ensures that $d\xi/dr$ is bounded as $r \to 0$.

For the above choice of $g(\xi)$, ξ, and $\tau(r, p)$, the transport Equation (23) reduces to the form

$$\frac{\partial^2 f_0}{\partial \eta^2} + \frac{1}{\eta}\frac{\partial f_0}{\partial \eta} + \frac{1}{5}\left(\frac{\partial^2 f_0}{\partial T^2} + (3+\alpha)\frac{\partial f_0}{\partial T}\right) = \frac{3N_0\delta(T)\delta(\xi - \xi_1)}{8\pi^2 p_0^3 c^2 \tau_0 g(\xi_1)}, \qquad (28)$$

where

$$\eta(r) = \xi_0 - \xi(r) = \xi_{02}\left(\frac{r}{r_2}\right)^k, \quad \xi_{02} = \xi_0 - \xi_2, \ \ g(\xi_1) = k(\xi_1 - \xi_0), \quad T = \ln\left(\frac{p}{p_0}\right). \qquad (29)$$

Figure 1 shows a plot of the fluid velocity $\beta(r) = u(r)/c$ versus r/r_2 based on the transformation in Equation (21) (see Webb et al. 2019), namely

$$\beta(r) = \tanh(\xi), \qquad \xi(r) = \xi_0 - \xi_{02}\left(\frac{r}{r_2}\right)^k, \qquad (30)$$

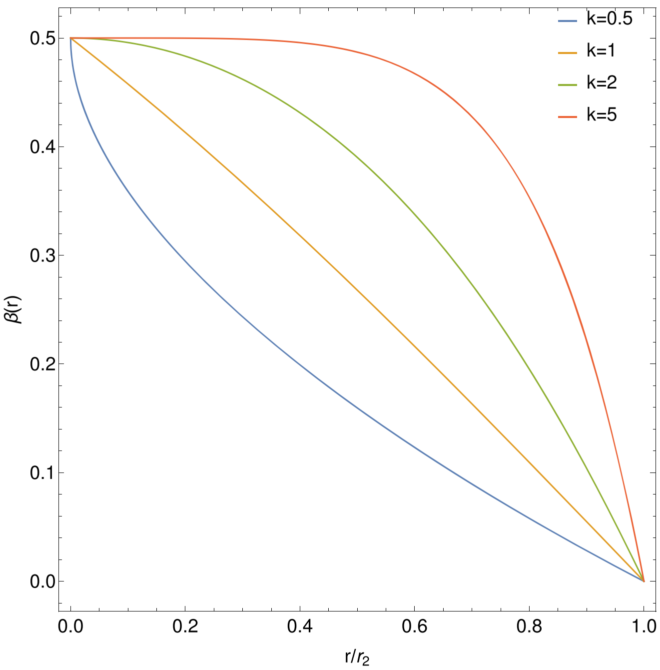

Figure 1. Velocity profile of $\beta(r) = u(r)/c$ vs. r/r_2 for jet shear acceleration problem. Parameter $k = 0.5,\ 1,\ 2,\ 5$ controls the $u(r)$ profile of the jet.

for $k = 0.5,\ 1,\ 2,\ 5$ for a jet with $\beta_0 = 0.5$ and $\beta_2 = 0$. The fluid velocity profile has a finite nonzero radial derivative $d\beta/dr$ at $r = 0$ for $k = 1$. Also note that $d\beta/dr = 0$ for $k > 1$ at $r = 0$ and $d\beta/dr \to -\infty$ as $r \to 0$ for $k < 1$ (i.e., a cusp for $0 < k < 1$). The fluid velocity profile for large k is relatively flat at small r but develops a steep shear layer near $r = r_2$ for the larger k cases. This turns out to be an interesting feature of the fluid velocity profile when we consider the effects of scattering on the particle acceleration in $r > r_2$ in which $\epsilon = k/s$ ($s = d\ln\tau/d\ln r$ in $r > r_2$) is a key parameter determining the hardness of the particle momentum spectrum of the accelerated particles.

In Sections 3 and 4, we obtain solutions of the transport Equation (28) for $f_0(r, p)$ that use the mixed boundary condition of Equations (14) or (17) for f_0. These solutions illustrate a substantially more effective acceleration of the particles because particles that have exited the shear flow region $0 < r < r_2$ may be scattered back into the shear flow region to be further accelerated by the flow.

3. Mixed Boundary Conditions Green's Function

In order to solve the mixed Dirichlet–Von Neumann boundary value problem of Equation (17), i.e.,

$$f_0(r_2, p) + \frac{r_2}{s}\frac{\partial f_0(r_2, p)}{\partial r} = f_0(\infty, p), \tag{31}$$

for the transport Equation (28) for $f_0(r, p)$, and also requiring that the diffusive particle flux $rS_d \to 0$ as $r \to 0$ (Equation (20)), it turns out that it is useful to find the solution f_G of the transport Equations (6) or (28) with a delta function source in Equation (7) satisfying the homogeneous version of the boundary condition of Equation (31) with $f_0(\infty, p) = 0$, i.e., f_G satisfies the boundary condition

$$f_0(r_2, p) + \frac{r_2}{s}\frac{\partial f_0(r_2, p)}{\partial r} = 0, \tag{32}$$

at the edge of the jet at radius $r = r_2$. This generalizes the homogeneous boundary condition $f_G(r_2, p; r_1, p) = 0$ used by Webb et al. (2018a, 2019) in solving the transport equation in which f_0 is specified on the boundary at $r = r_2$.

3.1. The Green's Function Solution

To obtain the Green's function solution satisfying the mixed boundary condition (32) at $r = r_2$, we search for solutions of the transport Equation (28) in (η, T) coordinates. We assume a scattering mean free time

$$\tau = \tau_0\left(\frac{p}{p_0}\right)^{\alpha} H(r_2 - r) + \tau_0\left(\frac{p}{p_0}\right)^{\alpha}\left(\frac{r}{r_2}\right)^{s} H(r - r_2). \tag{33}$$

We use the variables η and T to describe the solution, i.e.,

$$\eta = \xi_0 - \xi = \eta_2\left(\frac{r}{r_2}\right)^{k}, \quad \eta_2 \equiv \xi_{02}, \quad T = \ln\left(\frac{p}{p_0}\right). \tag{34}$$

Following the approach of Webb et al. (2019, their Appendix A), (144) et seq., suggests that we use the ansatz

$$f_G = \sum_{n=1}^{\infty} J_0(\lambda_n\eta)h_n(T), \tag{35}$$

where the values of λ_n are chosen to ensure that the boundary condition of et seq. (32) is satisfied and that f_G satisfies the transport Equation (28).

Substitution of the solution ansatz of Equation (35) into the mixed boundary condition of Equation (32) at $r = r_2$ and equating the coefficients of $h_n(T)$ to zero gives the eigenvalue equation

$$F(\lambda_n) = J_0(\lambda_n\eta_2) - \frac{k}{s}(\lambda_n\eta_2)J_1(\lambda_n\eta_2) = 0, \tag{36}$$

where we have used the result

$$J_0'(x) = -J_1(x), \tag{37}$$

(Abramowitz & Stegun 1965, formula 9.1.28, p. 361). The eigenvalue Equation (36) can also be expressed in the forms

$$J_0(j_n) - \epsilon j_n J_1(j_n) \equiv J_0(j_n) + \epsilon j_n J_0'(j_n) = 0, \quad n = 1, 2, \ldots, \tag{38}$$

where we use the notation

$$j_n = \lambda_n\eta_2 \quad \text{and} \quad \epsilon = \frac{k}{s}. \tag{39}$$

In the limit as $\epsilon \to 0$ (e.g., as $s \to \infty$), the eigenvalue Equation (38) reduces to the equation $J_0(j_n) = 0$. This case corresponds to the Dirichlet boundary condition $f_0 = 0$ at $r = r_2$, which is the free-escape boundary condition used by Webb et al. (2018a, 2019) in which it is implicitly assumed that $\kappa \to \infty$ in $r > r_2$.

It is instructive to note that for small ϵ $(0 < \epsilon \ll 1)$, Equation (38) can be written approximately in the form

$$J_0(j_n + \epsilon j_n) + O(\epsilon^2) = 0. \tag{40}$$

Hence, for small ϵ,

$$j_n(1+\epsilon) \approx j_{0,n} \quad \text{or} \quad j_n \approx \frac{j_{0,n}}{1+\epsilon}, \tag{41}$$

where $J_0(j_{0,n}) = 0$ defines the real positive zeros $\{j_{0,n}\}$ of $J_0(z)$. In Equation (41), $j_n < j_{0,n}$, and in particular $j_1 < j_{0,1}$, which, from Equation (52) for the asymptotic spectral index, μ_∞ implies hardening of the momentum spectrum of the accelerated particles compared to the free-escape boundary case.

The parameter $\epsilon = k/s$ in Equation (41) depends on the constant k, where

$$k = \frac{\partial \ln \eta}{\partial \ln r} \equiv -\frac{\gamma^2}{\eta}\frac{\partial \beta}{\partial \ln r}, \tag{42}$$

where

$$\xi = \frac{1}{2}\ln\left(\frac{1+\beta}{1-\beta}\right) \quad \text{and} \quad \eta = \xi_0 - \xi. \tag{43}$$

Thus,

$$\epsilon = \frac{k}{s} \equiv \frac{(\partial \ln \eta/\partial \ln r)H(r_2 - r)}{(\partial \ln \tau/\partial \ln r)H(r - r_2)}. \tag{44}$$

The mixed Dirichlet–Von Neumann boundary condition of Equation (31) expressed in terms of $\eta(r)$ has the form

$$\left[f_0 + \epsilon\eta\frac{\partial f_0}{\partial \eta}\right]_{r=r_2} = f_0(\infty, p). \tag{45}$$

The Green's function solution of the steady-state transport Equation (28) in the shear flow region $0 < r < r_2$ corresponding to monoenergetic injection of particles with momentum $p = p_0$ at radius $r = r_1$, in which the scattering mean free times in the region $0 < r < r_2$ and in the region $r > r_2$ are given by Equation (33), and with no sources of particles on the axis of the jet at $r = 0$, can be expressed in the form

$$f_0 = D\left(\frac{p}{p_0}\right)^{-a}\sum_{n=1}^{\infty}\frac{J_0(\lambda_n\eta)J_0(\lambda_n\eta_1)\exp(-\chi_n|T|)}{[J_0(j_n)^2 + J_1(j_n)^2]\chi_n}, \tag{46}$$

where

$$D = \frac{15N_0}{8\pi^2 p_0^3 c^2 \tau_0 k \eta_2^2}, \quad \epsilon = \frac{k}{s}, \quad a = \frac{3+\alpha}{2}. \tag{47}$$

The parameters $\eta_1 = \eta(r_1)$ and $\eta_2 = \eta(r_2)$. $J_0(z)$ and $J_1(z)$ are ordinary Bessel functions of the first kind. The eigenvalues j_n satisfy the eigenvalue Equation (38), and the parameters λ_n and χ_n are related to the j_n via the equations

$$j_n = \lambda_n\eta_2, \quad \text{and} \quad \chi_n = \sqrt{a^2 + 5\lambda_n^2}. \tag{48}$$

The term in the denominator in Equation (46) involving Bessel functions may also be simplified using the eigenvalue Equation (38), namely,

$$\begin{aligned} J_0(j_n)^2 + J_1(j_n)^2 &\equiv J_1(j_n)^2(1 + \epsilon^2 j_n^2) \\ &\equiv J_0(j_n)^2(1 + 1/(\epsilon^2 j_n^2)). \end{aligned} \tag{49}$$

The limit as $\epsilon \to 0$ recovers the free-escape Green's function solution of Webb et al. (2019). An outline of the derivation of the Green's function solution of Equation (46) is given in Appendix A.

In the region $r > r_2$, the solution for $f_0(r, p)$ has the form

$$f_0(r, p) = f_0(r_2, p)\left(\frac{r_2}{r}\right)^s H(r - r_2). \tag{50}$$

Thus, in the region $r > r_2$, the particle momentum spectrum has the same form that it has at $r = r_2$, and $f_0 \to 0$ as $r \to \infty$. The spectrum $f_0(r_2, p)$ is obtained by setting $r = r_2$ in the solution of Equation (46).

From Equation (46), it follows that the asymptotic momentum spectrum $f_0(r, p)$ as $p \to \infty$ has the form

$$f_0 \propto \left(\frac{p}{p_0}\right)^{-\mu_\infty} \quad \text{as} \quad p \to \infty, \tag{51}$$

where

$$\mu_\infty = a + \chi_1 \equiv a + (a^2 + 5j_1^2/\eta_2^2)^{1/2}. \tag{52}$$

For small ϵ, $j_1 \approx j_{0,1}/(1+\epsilon)$ (see Equation (41)) and Equation (52) gives

$$\mu_\infty \sim a + \{a^2 + 5j_{0,1}^2/[\eta_2^2(1+\epsilon)^2]\}^{1/2}, \tag{53}$$

which shows there is a spectral hardening of f_0 compared to the free-escape boundary case of Webb et al. (2019) for which $\epsilon = 0$. In Equations (46) and (52)

$$\begin{aligned} &\eta = \xi_0 - \xi, \quad \xi = \frac{1}{2}\ln\left(\frac{1+\beta}{1-\beta}\right), \\ &\eta_2 = \xi_{02} \equiv \frac{1}{2}\ln\left(\frac{1+\beta_{02}}{1-\beta_{02}}\right), \quad \beta_{02} = \frac{\beta_0 - \beta_2}{1 - \beta_0\beta_2}, \end{aligned} \tag{54}$$

where $\beta_0 = \beta(0)$ and $\beta_2 = \beta(r_2)$. Thus, the asymptotic spectral index in Equation (52) depends on the central velocity of the jet β_0 and also on the velocity of the jet at $r = r_2$ (in most applications, we set $\beta_2 = 0$ to simplify the discussion). The spectral index μ_∞ also depends critically on the parameter ϵ occurring in the eigenvalue Equation (38), which describes the effect of scattering outside the jet in the region $r > r_2$ (ϵ also depends on the shear velocity gradient of $\beta(r)$ or $u(r)$ in $0 < r < r_2$). Notice that β_{02} in Equation (54) is the relativistic relative velocity of the central jet velocity β_0 to the fluid velocity β_2 at the edge of the jet at $r = r_2$.

In the limit as $\epsilon \to 0$, the spectral index μ_∞ is the same as that given by Webb et al. (2019), in which j_1 is the first zero of $J_0(x)$. In the opposite limit as $\epsilon \to \infty$, Equation (52) gives

$$\mu_\infty \to 2a \equiv (3 + \alpha) \tag{55}$$

(here for large ϵ, the eigenvalue Equation (38) gives $J_1(j_1) \approx 0$, which implies $j_1 \to 0$ as $\epsilon \to \infty$). The spectral index $\mu_\infty = (3 + \alpha)$ is that obtained by Berezhko (1981), Berezhko & Krymsky (1981), and also by Rieger & Duffy (2006) for the case of space independent solutions for particle acceleration in shear flows. The case where $\epsilon = 0$ corresponds to a Dirichlet boundary condition applied at $r = r_2$, and the case where $\epsilon \to \infty$ corresponds to a Von-Neumann boundary condition at $r = r_2$. In the latter case, the spectral index of the accelerated particles at large momenta $p \gg p_0$ corresponds to the spectral index $\mu_\infty = (3 + \alpha)$. In general, the spectral index μ_∞ lies

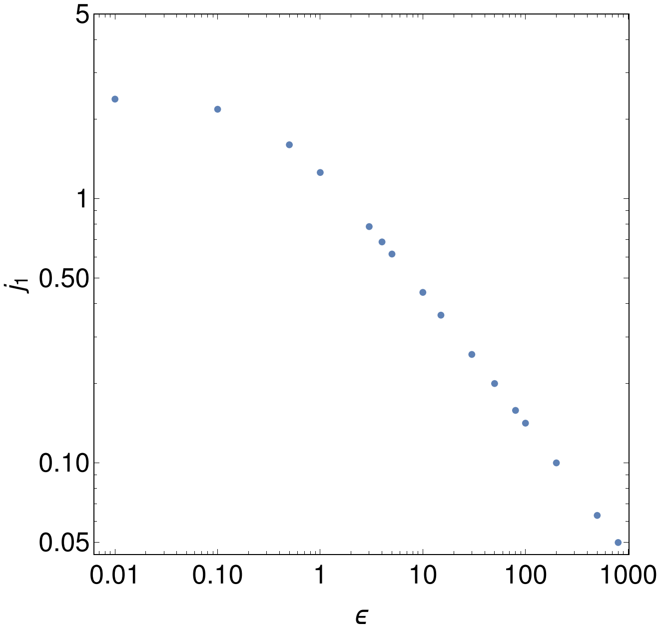

Figure 2. Eigenvalue j_1 vs. ϵ for eigenvalue Equation (38), which determines in part the asymptotic spectral index μ_∞ in Figure 3.

between the $\epsilon = 0$ limit and the $\epsilon \to \infty$ cases, and μ_∞ decreases (harder momentum spectra) as ϵ increases, and μ_∞ depends both on β_0 (the jet speed) and on ϵ.

Figure 2 shows the solution of the eigenvalue Equation (38) for the first eigenvalue j_1 as a function of ϵ. For $\epsilon = 0$, $j_1 \equiv j_{0,1} = 2.4048$, which is the first positive zero of $J_0(z)$, i.e., $J_0(j_{0,1}) = 0$. As ϵ increases, j_1 decreases to zero as $\epsilon \to \infty$. $j_1(\epsilon)$ plays an important role in determining the asymptotic spectral index μ_∞ in Equation (52) in encapsulating the dependence of the spectral index on the effects of diffusive scattering of particles outside the jet in $r > r_2$, providing a mechanism for the particles to reenter the shear flow in $0 < r < r_2$.

Figure 3 shows the asymptotic spectral index of particles accelerated in the shear flow as a function of the jet speed β_0 (we assume that $\beta_2 = 0$ for simplicity), for different values of the parameter ϵ. The case $\epsilon = 0$ corresponds to the case where particles freely escape from the shear flow. This means either $f = 0$ at $r = r_2$ or $f(r_2, p) = f(\infty, p)$, and this is a Dirichlet boundary condition where $\kappa \to \infty$ in $r > r_2$. In the limit as $\epsilon \to \infty$, $\mu_\infty \to 3 + \alpha$, which is the spectral index obtained by Berezhko (1982) and Rieger & Duffy (2006) from the analysis of the space independent Green's function solution at large times t. This case corresponds to the limit as $s \to 0$ where $\tau = \tau_0(p/p_0)^\alpha(r/r_2)^s$ in $r > r_2$. This, at first glance, seems innocuous, but it effectively means that particles cannot escape to infinity for $s = 0$. For each finite ϵ, the curve of μ_∞ versus β_0 asymptotes to $3 + \alpha$ as $\beta_0 \to 1$. For decreasing β_0, there is a value of β_0 for which μ_∞ becomes very large, and acceleration by shear is not very effective at producing high-energy particles. However, the hardness of the accelerated particle spectrum increases (i.e., μ_∞ decreases) as ϵ increases.

It is useful to keep in mind the behavior of the fluid velocity $u(r)$ dependence on the parameter k in Figure 1. It appears that for $k \gg 1$, the fluid velocity profile steepens and is relatively flat for most r in the region $0 < r < r_2$ but then falls steeply near $r = r_2$ (i.e., for large k there is a relatively thin shear layer

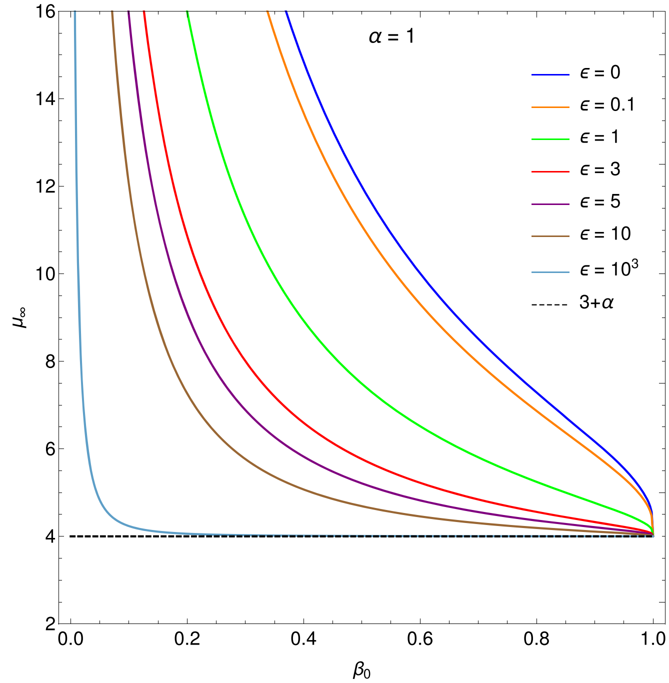

Figure 3. Spectral index μ_∞ for $f_0(r, p)$ as $p \to \infty$ ($f_0 \propto p^{-\mu_\infty}$), for $\alpha = 1$ ($\tau \propto p^\alpha$) vs. flow speed β_0 at $r = 0$ for a range of ϵ ($\epsilon = 0, 1, 5, 10, 10^3, \infty$) (we assume $\beta_2 = 0$). The curve for $\epsilon \to \infty$ is $\mu_\infty = 3 + \alpha$.

at the edge of the jet in which $u(r)$ falls precipitously to $u = u_2 = \beta_2 c$ at $r = r_2$ (in Figures 1 and 3, $\beta_2 = 0$)). Thus, one can obtain hard spectra for $\epsilon = k/s \gg 1$ in the cases (i) $k \gg 1$ and $s \approx 1$ say or if (ii) $k \sim 1$ and $s \sim 0$. Of course, $\epsilon \gg 1$ if $k \gg 1$ and s is small will give the largest possible ϵ. One should also keep in mind that the diffusion approximation used in the derivation of the diffusive transport equation assumes that the particle mean free path $\lambda \ll L$, where L is the characteristic scale of variation of the background flow.

3.2. Rieger & Duffy (2019) Leaky Box Model

Rieger & Duffy (2019) have discussed the spectral index μ_∞ of cosmic-rays in relativistic radio-jet shear flows on the basis of a leaky box model of particle acceleration and escape from the leaky box. In the leaky box model, the particle distribution function is assumed to be space independent. The escape of the particles from the box on a characteristic timescale $t_{\rm esc}$ takes into account the loss of particles from the box and represents particle transport out of the box due to advection or diffusion. In the steady-state case, Rieger & Duffy (2019) use the leaky box transport equation:

$$-\frac{1}{p^2}\frac{\partial}{\partial p}\left(\Gamma p^4 \tau \frac{\partial f_0}{\partial p}\right) = -\frac{f_0}{t_{\rm esc}}, \tag{56}$$

where $-f_0/t_{\rm esc}$ represents particle escape from the leaky box. An estimate for the escape time in the present case can be obtained from the formula

$$\kappa_\perp \equiv \kappa = \left\langle \frac{(\Delta r)^2}{2\Delta t} \right\rangle, \quad \kappa_\perp = \kappa_0\left(\frac{p}{p_0}\right)^\alpha, \quad \kappa_0 = \frac{c^2\tau_0}{3}, \tag{57}$$

from which it follows that

$$t_{\rm esc} = t_{\rm esc}^0\left(\frac{p}{p_0}\right)^{-\alpha}, \quad t_{\rm esc}^0 = \frac{3}{2}\left(\frac{r_2^2}{c^2}\right)\frac{1}{\tau_0}. \tag{58}$$

Here, we take $\Delta r = r_2$, and $t_{\rm esc} \equiv \Delta t$, which is obtained by solving (57) for Δt. For particle acceleration in a shear flow described by Equation (56), we may write

$$\begin{aligned} -\frac{1}{p^2}\frac{\partial}{\partial p}\left(\Gamma p^4 \tau \frac{\partial f_0}{\partial p}\right) &= \frac{1}{p^2}\frac{\partial}{\partial p}\left(\left\langle\frac{\Delta p}{\Delta t}\right\rangle p^2 f_0\right) \\ &- \frac{1}{p^2}\frac{\partial^2}{\partial p^2}\left(\left\langle\frac{(\Delta p)^2}{2\Delta t}\right\rangle p^2 f_0\right), \end{aligned} \tag{59}$$

where

$$\left\langle\frac{(\Delta p)^2}{2\Delta t}\right\rangle = \Gamma p^2 \tau, \quad \left\langle\frac{\Delta p}{\Delta t}\right\rangle = \frac{1}{p^2}\frac{\partial}{\partial p}(\Gamma p^4 \tau), \tag{60}$$

give the momentum space diffusion (dispersion) coefficient $\langle(\Delta p)^2/(2\Delta t)\rangle$ and the mean momentum gain coefficient $\langle \Delta p\rangle/\Delta t$ as measured in the local fluid frame. From Equation (60), we obtain the formula

$$t_{\rm acc} = \frac{p}{\langle \Delta p/\Delta t\rangle} = \frac{1}{(4+\alpha)\Gamma\tau}. \tag{61}$$

Equations (58) and (61) give

$$\frac{t_{\rm acc}}{t_{\rm esc}} = \frac{1}{(4+\alpha)\Gamma\tau_0 t_{\rm esc}^0}, \tag{62}$$

as the ratio of the mean acceleration time to the escape time for the leaky box model in Equation (56).

For effective acceleration, we require $t_{\rm acc}/t_{\rm esc} \ll 1$ (i.e., fast acceleration and slow escape). In the opposite case, $t_{\rm acc}/t_{\rm esc} \gg 1$, the particles escape the system before they can be accelerated, and one then expects a very steep momentum spectrum (soft spectrum) of particles. However, if $t_{\rm acc}/t_{\rm esc} \ll 1$, one expects a hard spectrum of particles accelerated by the shear. By substituting the solution ansatz $f_0 \propto p^{-\mu}$ in Equation (56) and using Equation (62), we obtain the quadratic equation

$$\mu^2 - (3+\alpha)\mu - (4+\alpha)t_{\rm acc}/t_{\rm esc} = 0, \tag{63}$$

with solutions

$$\mu = a \pm [a^2 + (4+\alpha)t_{\rm acc}/t_{\rm esc}]^{1/2} \quad \text{where} \quad a = \frac{(3+\alpha)}{2}. \tag{64}$$

From Equation (64), we obtain the asymptotic spectral index μ_∞ for large $p \gg p_0$ as

$$\mu_\infty = a + [a^2 + (4+\alpha)t_{\rm acc}/t_{\rm esc}]^{1/2}, \tag{65}$$

which resembles the formula (52) for μ_∞ obtained from the Green's function solution (46).

From Equations (5) and (58), we obtain

$$(4+\alpha)\frac{t_{\rm acc}}{t_{\rm esc}} = \frac{1}{\Gamma\tau_0 t_{\rm esc}^0} = \frac{10}{r_2^2\gamma^4(d\beta/dr)^2}. \tag{66}$$

This expression is slightly different from that used by Rieger & Duffy (2019), as we have not approximated $d\beta/dr$ as they did. To proceed further, it is necessary to find an averaged value of $\gamma^4(d\beta/dr)^2$ across the jet. We use the physically intuitive approximation

$$\left\langle \gamma^4\left(\frac{d\beta}{dr}\right)^2\right\rangle = \left\langle \gamma^2\left(\frac{d\beta}{dr}\right)\right\rangle^2, \tag{67}$$

where the angle brackets denote a spatial average across the jet. We obtain

$$\left\langle \gamma^2\frac{d\beta}{dr}\right\rangle = -\frac{1}{2r_2}\ln\left(\frac{1+\beta_{02}}{1-\beta_{02}}\right), \tag{68}$$

Using Equations (66) and (68) in Equation (65) gives

$$\mu_\infty^{\rm RD} \equiv \mu_\infty = a + \left\{a^2 + 40\left[\ln\left(\frac{1+\beta_{02}}{1-\beta_{02}}\right)\right]^{-2}\right\}^{1/2}, \tag{69}$$

which is essentially the expression for μ_∞ obtained by Rieger & Duffy (2019; they set $\beta_2 = 0$ in their analysis).

The expression in Equation (69) for μ_∞ is similar to the expression for μ_∞ obtained by Webb et al. (2018a), Equation (67) (which used a different prescription for the scattering time $\tau(r, p)$ than that used in the present paper), namely,

$$\mu_\infty^{(18)} = a + \left\{a^2 + 5\pi^2\left[\ln\left(\frac{1+\beta_{02}}{1-\beta_{02}}\right)\right]^{-2}\right\}^{1/2}. \tag{70}$$

The results of Equations (69) and (70) have the same functional dependence on β_{02} and give approximately the same values (see, e.g., Rieger & Duffy 2019). The results of Webb et al. (2018a, 2019) assumed that there was no particle scattering outside the jet shear flow region $0 < r < r_2$. The results of Equations (69) and (70) have a similar form to the result for μ_∞ in Equation (52), which can be written in the form

$$\mu_\infty = a + \left\{a^2 + 20 j_1(\epsilon)^2\left[\ln\left(\frac{1+\beta_{02}}{1-\beta_{02}}\right)\right]^{-2}\right\}^{1/2}. \tag{71}$$

This expression differs from Equations (69) and (70) for μ_∞ in that it depends on the parameter ϵ, which describes the effect of particle scattering outside the shear flow region $0 < r < r_2$ (ϵ also describes in part the effect of the gradient of the shear flow in $0 < r < r_2$). For the case of no scattering in $r > r_2$, $\epsilon = 0$. In this case, $j_1 \equiv j_1(0)$ is the first zero of $J_0(x)$, i.e., $j_1 \sim 2.4048$, and $20 j_1(0)^2 = 115.66$. This value of the constant in front of the log term is about three times that in Equation (69).

By comparing the expressions in Equation (65) for μ_∞ in the leaky box model with the expression for μ_∞ from Equation (71), we obtain the expression

$$\frac{t_{\rm acc}}{t_{\rm esc}} = \frac{20 j_1(\epsilon)^2}{(4+\alpha)}\left[\ln\left(\frac{1+\beta_{02}}{1-\beta_{02}}\right)\right]^{-2} \equiv \frac{5 j_1(\epsilon)^2}{(4+\alpha)\eta_2^2}, \tag{72}$$

for the ratio of the acceleration time $t_{\rm acc}$ to the escape time $t_{\rm esc}$ for particle acceleration in radio-jet shear flows.

3.2.1. The Parameter ϵ

The parameter $\epsilon = k/s$ represents both acceleration and escape or confinement effects. The parameter k

$$k = \frac{\partial \ln \eta}{\partial \ln r}, \tag{73}$$

describes the velocity profile in the shear flow region $0 < r < r_2$. Note that

$$k = \frac{\gamma^2}{\eta} r \left| \frac{d\beta}{dr} \right|, \quad \eta = \xi_0 - \xi, \quad \xi = \frac{1}{2} \ln\left(\frac{1+\beta}{1-\beta}\right) \tag{74}$$

depends on the flow velocity gradient $|d\beta/dr|$ and also on $\beta(r)$.

The parameter s depends on the radial dependence of the diffusion coefficient or the mean scattering time τ in the region $r > r_2$. If we define

$$\langle \nu(r_2, p; R) \rangle = \int_{r_2}^{R} \frac{dr'}{r'\tau(r', p)} \equiv \frac{c^2}{3} \int_{r_2}^{R} \frac{dr'}{r'\kappa(r', p)}, \tag{75}$$

and use the ansatz $\tau = \tau_0 \bar{p}^{\alpha} (r/r_2)^s$ in $r > r_2$ in Equation (75), we obtain

$$\langle \nu(r_2, p; R) \rangle = \frac{1}{\tau_0 \bar{p}^{\alpha}} \begin{cases} (1/s)[1 - (R/r_2)^{-s}] & \text{if} \quad s > 0, \\ \ln(R/r_2) & \text{if} \quad s = 0 \end{cases}. \tag{76}$$

From Equation (76),

$$\langle \nu(r_2, p; \infty) \rangle = \frac{1}{s\tau_0} (\bar{p})^{-\alpha} \quad \text{where} \quad \bar{p} = \frac{p}{p_0}. \tag{77}$$

where we assume $s > 0$. Hence,

$$\langle \nu(r_2, p_0; \infty) \rangle = \frac{1}{s\tau_0} \quad \text{and} \quad s = \frac{1}{\langle \nu(r_2, p_0; \infty) \rangle \tau_0}. \tag{78}$$

Thus, we can identify $s = \langle \tau \rangle / \tau_0$ where $\langle \tau \rangle = 1/\langle \nu \rangle$ is the mean scattering time in $r > r_2$ at momentum $p = p_0$. Thus, small s corresponds to strong scattering in $r > r_2$. In other words, $s \to 0$ as $\langle \tau \rangle \to 0$ corresponds to strong scattering in $r > r_2$. This also implies that for a fixed k, $\epsilon \to \infty$ as $s \to 0$. Note that in Equation (76), $\langle \nu(r_2, p_0; R) \rangle$ is well defined for $s = 0$ and $\langle \nu(r_2, p_0; R) \rangle \to \infty$ as $R \to \infty$.

For fixed k, $\epsilon = k/s$ measures how the particle mean free path and diffusion coefficient increase with distance r outward from $r = r_2$ due to a dying off of the turbulence scattering the particles with increasing r. Thus, ϵ in this formulation describes the evolution and decay of turbulence outside the shear layer, which presumably can be quantified by observations of radio jets. Furthermore, it should be possible, based in part on observations comparing the flow kinetic energy of the jet, and whether it is sufficient to power the cosmic-rays (see Axford 1981), for a similar calculation carried out to determine if the galactic cosmic-rays can be powered by supernova remnant shocks in the hot interstellar medium. Axford (1994) discusses acceleration mechanisms for the UHECR spectrum.

To sum up, the Rieger & Duffy (2019) analysis yields physical insight into the role of the acceleration time $t_{\rm acc}$ and the escape time $t_{\rm esc}$ on the asymptotic spectral index μ_∞ of shear accelerated particles in radio jets, but the details of the exact value of μ_∞ change depending on the detailed form of the particle scattering and the shear velocity profile of the jet.

We investigate further the above leaky box model for the spectral index μ_∞ in Section 5, where we include the effects of synchrotron losses on the asymptotic particle momentum spectrum of the particles for the case $\alpha = 1$ and use the analysis to discuss active galactic nucleus jet examples.

3.3. Green's Function Characteristics

Figure 4 shows plots of $\mathrm{Log}(f_0/D)$ versus $\mathrm{Log}(p/p_0)$ for the Green's function solution in Equation (46) at the source radius $r = r_1$, $\beta = \beta_1 = 0.1$. In the left panel, $\beta_0 = 0.3$, 0.4, 0.6, 0.8 and 0.99, and $\epsilon = 0$ (free escape at $r = r_2$). The left panel is the same as that in Figure 4 of Webb et al. (2019). In the right panel, $\beta_0 = 0.3$, 0.4.0.6, 0.8, 0.99 and $\epsilon = 1$. The parameters $\beta_2 = 0$ and $\alpha = 1$. The main point to note is the spectral hardening of the solution as ϵ increases from $\epsilon = 0$ (left panel) to $\epsilon = 1$ (right panel).

Figure 5 shows plots of $\mathrm{Log}(f_0/D)$ versus $\mathrm{Log}(p/p_0)$ for the Green's function solution in Equation (46) on the axis of the jet ($\beta = \beta_0 = 0.5$) for a range of injection radii ($\beta_1 = 0.001$, 0.01, 0.2, and 0.5). The parameters $\beta_2 = 0$, $\alpha = 1$, and $\epsilon = 1$. The left panel corresponds to the $\epsilon = 0$ case studied by Webb et al. (2019) with a free-escape boundary at $r = r_2$. The right panel corresponds to $\epsilon = 1$, which is a mixed Dirichlet–Von Neumann boundary condition case, in which particles can scatter back into the shear flow from the region $r > r_2$. Note the harder momentum spectra for the $\epsilon = 1$ case (right panel). The spectra on the right panel for different β_1 lie very close together compared to the spectra in the left panel with $\epsilon = 0$, indicating perhaps that the particles find it more difficult to escape for the $\epsilon = 1$ case. The particle spectra for momenta $p < p_0$ are also more decelerated for the $\epsilon = 1$ case compared to the $\epsilon = 0$ case.

Figure 6 shows $\log(f_0/D)$ versus $\log(p/p_0)$ at radius $r = r_2$ where $\beta_2 = 0$, for the Green's function solution in Equation (46) for a jet with $\beta_0 = 0.6$ and $\alpha = 1$, for the cases $\epsilon = 1$ and $\epsilon = 5$. The left panel is for the case $\beta_1 = 0.1$, and the right panel is for the case $\beta_1 = 0$. Note that the right panel spectrum (Figure 6(b)) is sharply peaked about $p = p_0$, because in this case, the source is located on the boundary at $r = r_2$, whereas the spectra in Figure 6(a) is slightly rounded, because the source at $\beta = \beta_1 = 0.1$ (i.e., at $r = r_1$) is not located on the boundary at $r = r_2$ where $\beta_2 = 0$. Note the hardening of the spectrum as ϵ increases. The case $\epsilon = 0$ (not shown) corresponds to $f_0 = 0$ at $r = r_2$.

4. Boundary Value Problems

In this section, we use Green's formula (Webb et al. 2018a, 2019) to solve boundary value problems of the steady-state transport equation

$$\mathcal{L}(f_0) = -\frac{1}{r}\frac{\partial}{\partial r}\left(r\kappa \frac{\partial f_0}{\partial r}\right) - \frac{1}{p^2}\frac{\partial}{\partial p}\left(\Gamma p^4 \tau \frac{\partial f_0}{\partial p}\right) = Q(r, p). \tag{79}$$

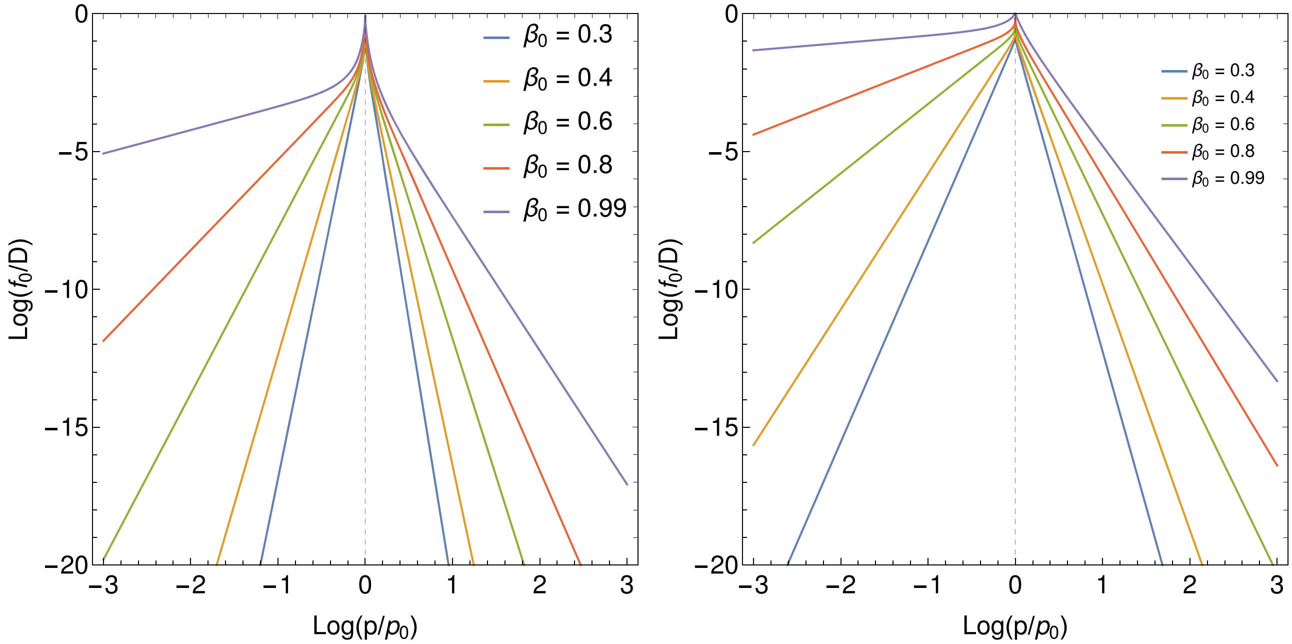

Figure 4. Plots of log (f_0/D) vs. log (p/p_0) distribution function spectra for the Green's function of Equation (46) at the source radius $r = r_1$ where $\beta = \beta_1 = 0.1$. Left panel: $\beta_0 = 0.3, 0.4, 0.6, 0.8, 0.99$, $\epsilon = 0$. Right panel: $\beta_0 = 0.3, 0.4, 0.6, 0.8, 0.99$ and $\epsilon = 1$. The other parameters are $\beta_2 = 0$, $\alpha = 1$. Notice that the spectrum hardens as ϵ increases.

From Webb et al. (2018a), the differential form of Green's theorem for the transport Equation (79) is the identity

$$\psi\mathcal{L}(f_0) - f_0\mathcal{L}^\dagger(\psi) = \mathcal{B}(\psi, f_0). \tag{80}$$

For the transport Equation (79), the adjoint transport equation operator $\mathcal{L}^\dagger$ is equivalent to $\mathcal{L}$, i.e.,

$$\mathcal{L}^\dagger = \mathcal{L}. \tag{81}$$

The bilinear concomitant $\mathcal{B}(\psi, f_0)$ is given by

$$\begin{aligned}\mathcal{B}(\psi, f_0) = &\frac{1}{r}\frac{\partial}{\partial r}\left[r\kappa\left(f_0\frac{\partial\psi}{\partial r} - \psi\frac{\partial f_0}{\partial r}\right)\right]\\ &+ \frac{1}{p^2}\frac{\partial}{\partial p}\left[\Gamma p^4\tau\left(f_0\frac{\partial\psi}{\partial p} - \psi\frac{\partial f_0}{\partial p}\right)\right],\end{aligned} \tag{82}$$

(e.g., Morse & Feschbach 1953, Vol. 1, p. 527–528). Note that $\mathcal{B}(\psi, f_0)$ is a pure divergence expression in (r, p)-space.

To obtain Green's formula, we introduce the adjoint Green's function

$$\Gamma(r', p'; r, p) \equiv \psi(r', p'), \tag{83}$$

where Γ satisfies the adjoint equation

$$\mathcal{L}'[\Gamma(r', p'; r, p)] = \frac{\delta(r' - r)\delta(p' - p)}{rp^2}, \tag{84}$$

where we used the fact that $\mathcal{L}$ is self adjoint. In Equation (84), the operator $\mathcal{L}'$ acts on the (r', p') variables, and (r, p) are the source variables. We choose $\Gamma(r', p'; r, p)$ to satisfy the boundary conditions

$$r'\kappa(r', p')\frac{\partial\Gamma(r', p'; r, p)}{\partial r'} \to 0 \quad \text{as} \quad r' \to 0, \tag{85}$$

$$\Gamma(r', p'; r, p) + \frac{r_2}{s}\frac{\partial\Gamma(r', p'; r, p)}{\partial r'}\Big|_{r'=r_2} = 0. \tag{86}$$

The boundary condition of Equation (86) is the same as the Dirichlet–Von Neumann boundary condition of Equation (32) used in obtaining the Green's function in Equation (48) of Section 3. The boundary condition of Equation (85) as $r \to 0$ is the same as in Equation (20), corresponding to no particles sources as $r \to 0$.

Following the approach of Webb et al. (2018a), Green's formula for the transport Equation (79) follows by integrating the differential Green's theorem of Equation (80) over the region

$$\mathcal{R} = \{(r, p): \quad 0 < r < r_2, \quad 0 < p < \infty\}, \tag{87}$$

(i.e., over the variables (r', p') in $\mathcal{R}$, with respect to $r'dr' \wedge (p'^2dp')$). The net result is Green's formula for $f_0(r, p)$ for $(r, p) \in \mathcal{R}$, namely,

$$\begin{aligned}f_0(r, p) \;=\; &\int_0^{r_2} r'dr' \int_0^\infty p'^2dp'\Gamma(r', p'; r, p)Q(r', p')\\ &+ \int_0^{r_2} r'dr'\left[\Gamma' p'^4\tau'\left(f_0'\frac{\partial\Gamma'}{\partial p'} - \Gamma'\frac{\partial f_0'}{\partial p'}\right)\right]_{p'=0}^{\infty}\\ &+ \int_0^\infty p'^2dp'\left[r'\kappa'\left(\Gamma'\frac{\partial f_0'}{\partial r'} - f_0'\frac{\partial\Gamma'}{\partial r'}\right)\right]_{r'=0}^{r_2}.\end{aligned} \tag{88}$$

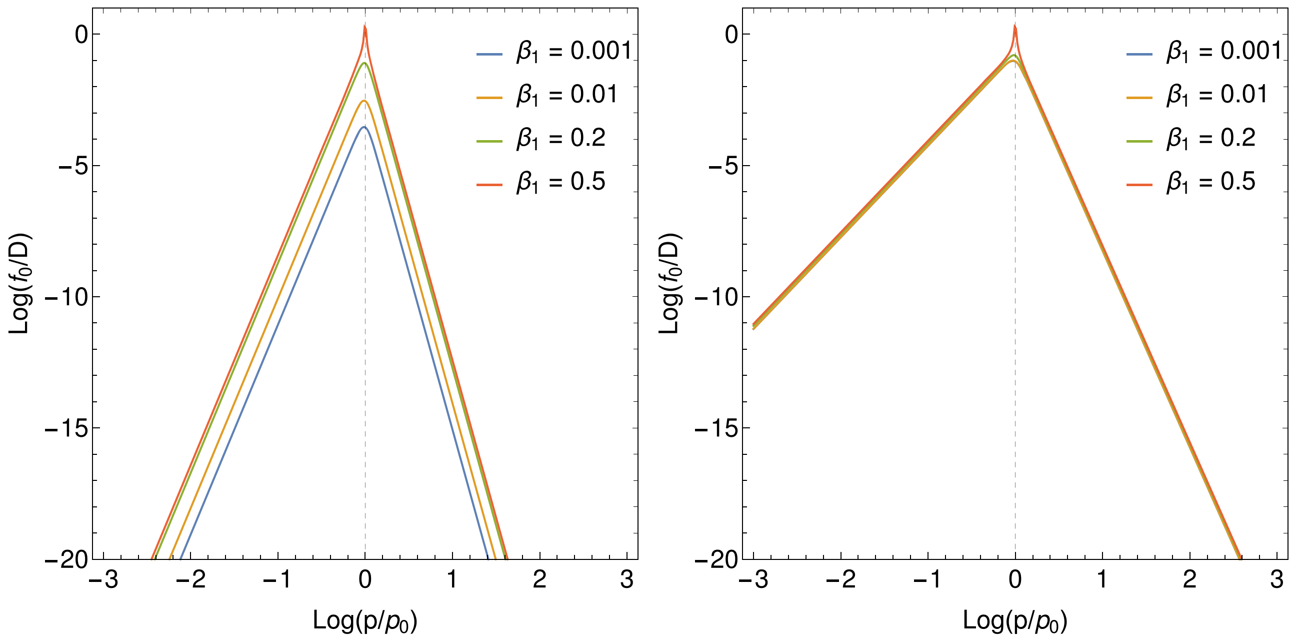

Figure 5. Plots of log (f_0/D) vs. log (p/p_0) distribution function spectra for the Green's function in Equation (46) at $r = 0$ where $\beta = \beta_0 = 0.5$, for a range of injection radii $r = r_1$ specified by β_1 ($\beta_1 = 0.001$, 0.01, 0.2, and 0.5). The parameters $\beta_2 = 0$ and $\alpha = 1$. The left panel corresponds to the free-escape boundary case $\epsilon = 0$ (see Webb et al. 2019). For the right panel, $\epsilon = 1$. Note the harder spectra for $\epsilon = 1$.

In the following, we assume that the spatial integral with limits from $p' = 0$ to $p' = \infty$ representing particle transport across the momentum boundaries is zero.

To proceed further with Green's formula in Equation (88), notice that by using the boundary condition of Equation (86) that

$$\begin{aligned}
&\left[r'\kappa(r', p')\left(\Gamma'(r', p'; r, p)\frac{\partial f_0'}{\partial r'}\right.\right.\\
&\left.\left.- f_0'(r', p')\frac{\partial\Gamma(r', p'; r, p)}{\partial r'}\right)\right]_{r'=r_2}\\
&\equiv\left[r'\kappa'\left\{\Gamma'\frac{\partial f_0'}{\partial r'} - f_0{}'\left[-\frac{s}{r_2}\Gamma(r', p'; r, p)\right]\right\}\right]_{r'=r_2}\\
&=\left\{r'\kappa\left(\frac{s}{r_2}\right)(\Gamma(r', p'; r, p)\right.\\
&\left.\times\left[\frac{r_2}{s}\frac{\partial f_0'}{\partial r'} + f_0(r', p')\right]\right)\Bigg\}_{r'=r_2}\\
&=\left[r'\kappa'\frac{s}{r_2}f_0(\infty, p')\Gamma(r', p'; r, p)\right]_{r'=r_2}\\
&=-\left[r'\kappa' f_0(\infty, p')\frac{\partial\Gamma(r', p'; r, p)}{\partial r'}\right]_{r'=r_2}.
\end{aligned} \tag{89}$$

Thus, the above integrand term in Equation (88) can be represented as $f_0(\infty, p')$ multiplied by either a $\Gamma(r', p'; r, p)$ term or by a $\partial\Gamma(r', p'; r, p)/\partial r'$ term at $r' = r_2$.

Assuming that there are no sources of particles in the region $0 < r < r_2$, we set $Q(r', p') = 0$ and obtain the Green's formula solution

$$\begin{aligned}
f_0 &= \int_0^\infty dp'\\
&\times\left[p'^2\frac{k}{\epsilon}\kappa(r', p')\Gamma(r', p'; r, p)f_0(\infty, p')\right]_{r'=r_2}\\
&\equiv -\int_0^\infty dp'\, p'^2 r_2\kappa(r_2, p)\\
&\times\left[\frac{\partial\Gamma(r', p'; r, p)}{\partial r'}\right]_{r'=r_2} f_0(\infty, p').
\end{aligned} \tag{90}$$

Both formulas in Equation (90) are equivalent because of the mixed Dirichlet–Von Neumann boundary conditions in Equation (86) at $r' = r_2$. In Equation (90), we assume that there is no contribution to the solution in Equation (88) for $f_0(r, p)$ from the lower boundary as $r' \to 0$. The second form for $f_0(r, p)$ in Equation (90) corresponds to the Green's formula for $f_0(r, p)$ given by Webb et al. (2019), Equation (60), for the case $\epsilon \to 0$.

To find the explicit form of the Green's function $\Gamma(r', p'; r, p)$ in Equation (90), we use the map

$$\frac{N_0}{8\pi^2} \to 1, \quad r \to r', \quad p \to p', \quad r_1 \to r, \quad p_0 \to p, \tag{91}$$

in the Green's function solution of Equation (46), to obtain the formula

$$\begin{aligned}
\Gamma(r', p'; r, p) &= \tilde{D}\exp[-aT(p', p)]\sum_{n=1}^\infty\\
&\times\frac{J_0(\lambda_n\eta)J_0(\lambda_n\eta')\exp(-\chi_n|T(p', p)|)}{[J_0(j_n)^2 + J_1(j_n)^2]\chi_n},
\end{aligned} \tag{92}$$

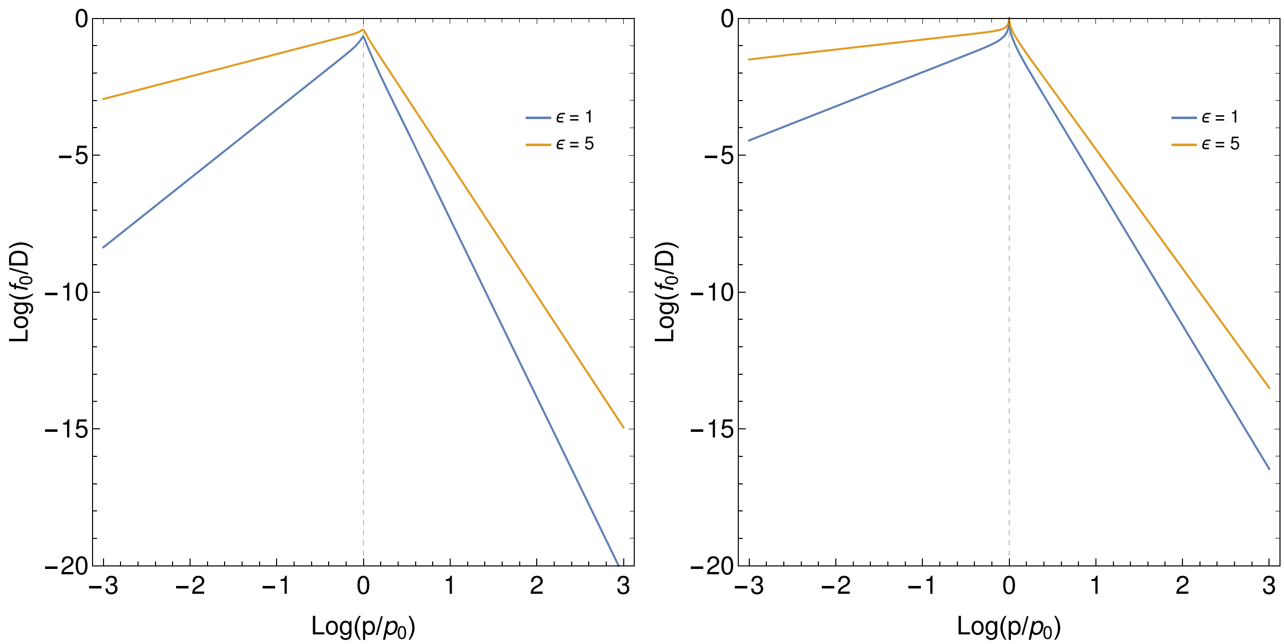

Figure 6. Plots of log (f_0/D) vs. log (p/p_0) for the Green's function in Equation (46) at $r = r_2$ where $\beta = \beta_2 = 0$. $\beta_0 = 0.6$, and ϵ has the values $\epsilon = 1$ and $\epsilon = 5$. $\alpha = 1$. Left panel: $\beta_1 = 0.1$; right panel: $\beta_1 = 0.0$.

where

$$\tilde{D} = \frac{15}{p^3(c^2\tau_0)k\eta_2^2}, \quad T(p_a, p_b) = \ln\left(\frac{p_a}{p_b}\right). \tag{93}$$

Here, the map in Equation (91) implies the transformation

$$\kappa(r, p) = \kappa_0\left(\frac{p}{p_0}\right)^\alpha \Rightarrow \kappa(r', p') = \kappa_0\left(\frac{p'}{p}\right)^\alpha. \tag{94}$$

As an example of the use of the Green's formula solution form in Equation (90) for $f_0(r, p)$ in the region $0 < r < r_2$, consider the case where

$$f_0(\infty, p) = \frac{N_g\delta(p - p_0)}{4\pi p_0^2}, \tag{95}$$

corresponding to a monoenergetic momentum spectrum of particles as $r \to \infty$. Substitution of Equations (92)–(95) into the Green's formula of Equation (90) gives the solution for $f_0(r, p)$ for the region $0 < r < r_2$ corresponding to a monoenergetic spectrum in Equation (95) at infinity of the form

$$f_0(r, p) = D_1\exp[-aT(p, p_0)]\sum_{n=1}^{\infty} \times \frac{j_nJ_1(j_n)J_0(\lambda_n\eta)\exp(-\chi_n|T(p, p_0)|)}{[J_0(j_n)^2 + J_1(j_n)^2]\chi_n}, \tag{96}$$

where

$$T(p, p_0) = \ln\left(\frac{p}{p_0}\right), \quad D_1 = \frac{5N_g}{4\pi\eta_2^2p_0^3}. \tag{97}$$

The solution of Equation (96) in the limit as $\epsilon \to 0$ reduces to the free-escape boundary monoenergetic spectrum solution obtained by Webb et al. (2019), Equation (58). In the solution of Equation (96), the eigenvalue Equation (40) applies, i.e.,

$$J_0(j_n) - \epsilon j_nJ_1(j_n) = 0, \quad n = 1, 2,\ldots. \tag{98}$$

Note that the values of j_n in Equation (98) depend on the parameter $\epsilon = k/s$ where $k = \partial\ln\eta/\partial\ln r$ in $0 < r < r_2$ and $s = \partial\ln\kappa/\partial r$ in the region $r > r_2$.

Using Equations (16) and (17), the solution for $f_0(r, p)$ in the region $r > r_2$ has the form

$$f_0(r, p) = f_0(\infty, p) - [f_0(\infty, p) - f_0(r_2, p)]\left(\frac{r}{r_2}\right)^{-s}, \tag{99}$$

where $f_0(\infty, p)$ is given by Equation (95), and $f_0(r_2, p)$ is obtained by setting $r = r_2$ in Equation (96).

4.1. Examples

Figure 7(a) shows a plot of $\log(f_0/D_1)$ versus $\log(p/p_0)$ for the monoenergetic spectrum solution of Equation (96) for the case $\epsilon = 0$, in which $f_0 \to N_g\delta(p - p_0)/(4\pi p_0^2)$ as $r \to \infty$. The central jet velocity $\beta_0 = 0.6$. The particle spectra are shown at the locations $\beta = 0.01$, 0.1, and 0.5. $\beta_2 = 0$ and $\alpha = 1$. For $\epsilon = 0$, the boundary $r = r_2$ is a free-escape boundary in which $f_0(r_2, p) = N_g\delta(p - p_0)$ at $r = r_2$. $\beta_2 = 0$ at $r = r_2$. The curve $\beta = 0.01$ is close to the boundary $r = r_2$. The number of particles increases as r decreases toward $r = 0$. Figure 7(b) shows similar plots of f_0 versus p/p_0 using a log scale on both axes, for the case $\epsilon = 1$. Notice that the distribution function curves are now much closer together, presumably because scattering outside the jet allows particles to reenter the shear flow acceleration region ($0 < r < r_2$) with concomitant enhanced particle acceleration. For $\epsilon = 1$, there is now a much harder power-law spectral index of the accelerated particles with $p > p_0$. Figure 7(c) shows similar plots for the case $\epsilon = 5$ and for $\beta_0 = 0.6$ and $\beta = 0.01$, 0.1, and 0.5. Again, f_0 increases with increasing β as one moves toward the center of the jet.

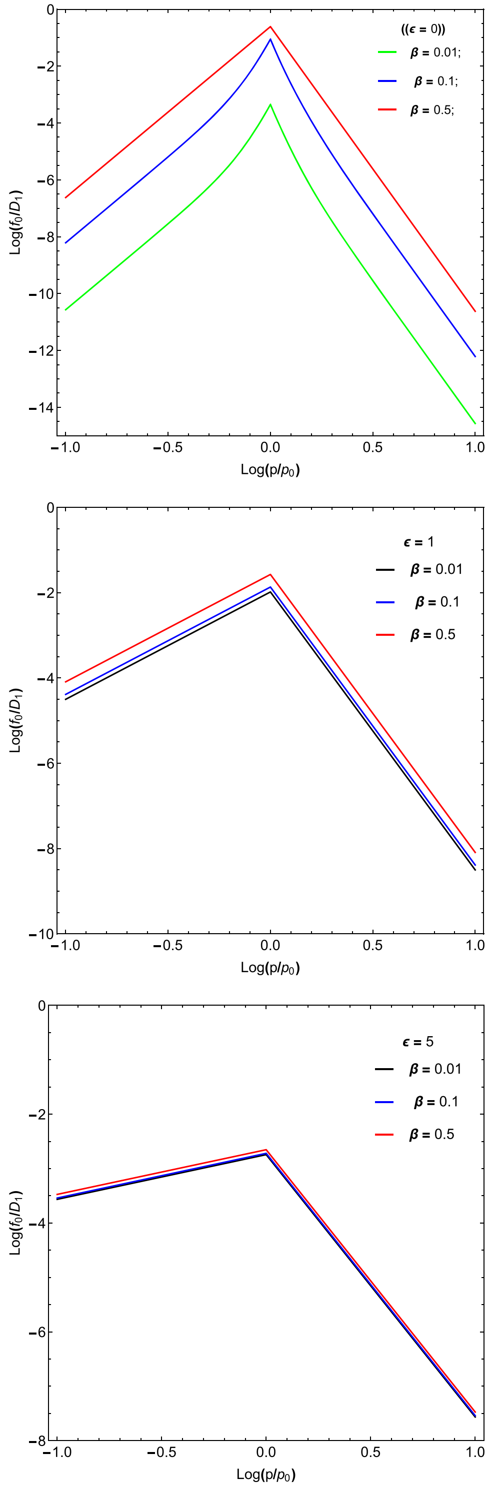

Figure 7. Plots of log (f_0/D_1) vs. log (p/p_0) distribution function spectra for a jet with a central velocity of $\beta_0 = 0.5$ at $r = 0$. The spectra are shown at the locations $\beta = 0.01$, 0.1, and 0.5 (note that $\beta(r)$ decreases with increasing r. Top panel: $\epsilon = 0$ corresponds to the free escape of particles at $r = r_2$ where $\beta = 0$. Middle panel: nonzero scattering in $r > r_2$ with $\epsilon = 1$. Bottom panel: $\epsilon = 5$ (scattering in $r > r_2$ increases as ϵ increases).

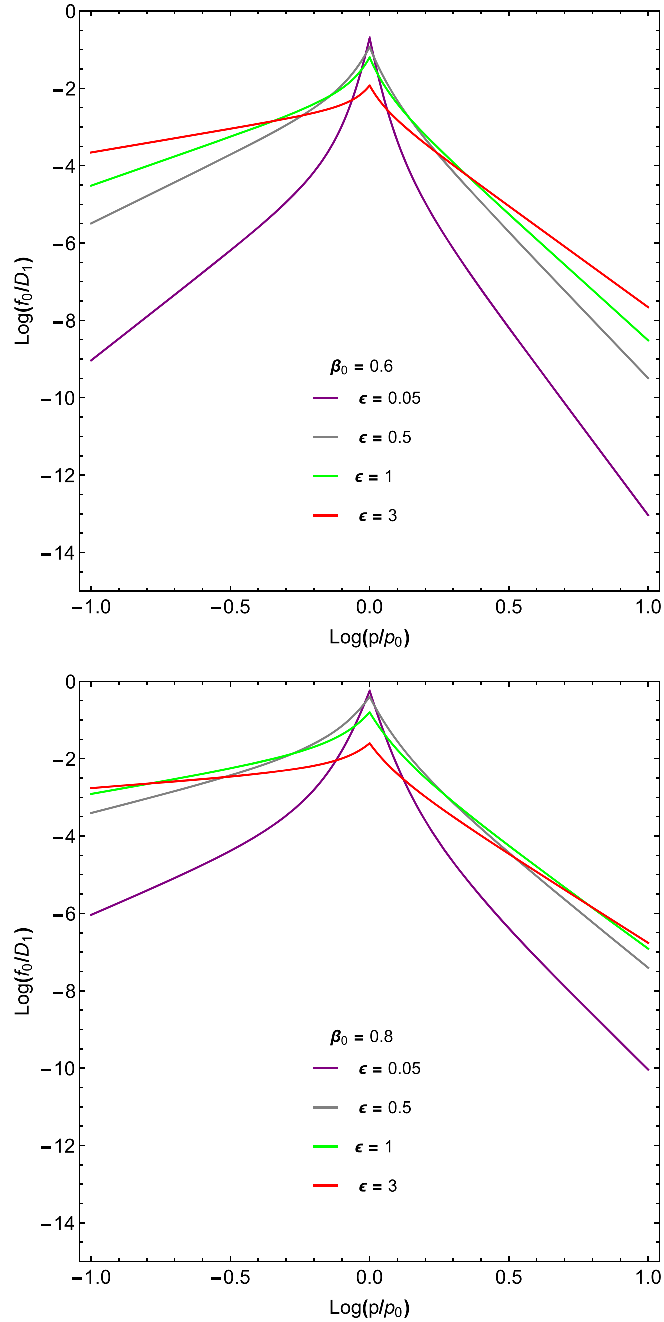

Figure 8. Top panel: plot of $\log(f_0/D_1)$ vs. $\log(p/p_0)$ on the shear flow boundary at $r = r_2$ for a jet with central velocity $\beta_0 \equiv \beta(0) = 0.6$ at $r = 0$, and $\beta_2 = \beta(r_2) = 0$. $\epsilon = 0.05$, 0.5, 1, 3. Bottom panel: same as the top panel, except that $\beta_0 = 0.8$.

Figures 8(a) and (b) show plots of f_0 versus p/p_0 using a log scale on both axes. Figure 8(a) shows the change in the distribution function at the shear flow boundary at $r = r_2$ where $\beta_2 = 0$. The central jet flow velocity $\beta_0 = 0.6$ and the parameter $\epsilon = 0.05$, 0, 5, 1, 3 in Figure 8(a). Figure 8(b) shows a similar plot of f_0 versus p/p_0 at $r = r_2$ for the case $\epsilon = 0.05, 0.5, 1, 3$ and $\beta_0 = 0.8$. The lowest amplitude for f_0 is obtained for $\epsilon = 0.01$. As ϵ increases to $\epsilon = 1$, there is a dramatic increase of the number of particles observed at the boundary $r = r_2$, but as ϵ increases further to $\epsilon = 5$, there is a decrease of f_0 at the boundary. The increase in f_0 for $\epsilon = 1$ occurs because the particles do not freely escape from the region $0 < r < r_2$ and are more effectively trapped because of scattering in $r > r_2$, which reflects the exiting particles back into $0 < r < r_2$. However, one needs to keep in mind that the particles in these solutions originate with momentum $p = p_0$ as $r \to \infty$. As ϵ increases to $\epsilon = 5$, the distribution function amplitude decreases, because for large enough ϵ, the particles are strongly scattered in the outer region $r > r_2$ and find it much harder to reach $r = r_2$ from infinity. Thus, it appears that for particles to be effectively accelerated by the shear flow, there is an optimum value of ϵ for particles to reach $r = r_2$ from infinity. Note also from Figure 3 that the accelerated particle spectrum hardens with increasing ϵ, but the particle number density on the $r = r_2$ boundary decreases for very large values of ϵ.

5. Discussion and Estimates

In this section, we discuss applications of the results obtained in Sections 3 and 4 to the acceleration of UHECR due to cosmic-ray viscosity and fluid shear in radio jets. It turns out that there are three timescales. To discuss the timescales involved, it is useful to study in more detail the time-dependent relativistic transport equations for cosmic-rays, based on the moment equations of Webb (1989). A derivation of the telegrapher transport equation obtained by Webb et al. (2018b; because of space limitations) will be provided elsewhere.

Section 5.1 describes the relativistic telegrapher equation and its form for cylindrical symmetry about the jet axis. Section 5.2 develops a leaky box model for particle acceleration in a relativistic jet shear flow, based in part on the work of Rieger & Duffy (2019). Section 5.3 discusses in the acceleration timescale $t_{\rm acc}$, the escape timescale $t_{\rm esc}$, and the synchrotron loss timescale and their role in determining the spectrum of the accelerated particles in the leaky box model. Section 5.4 provides timescale estimates for particle acceleration, synchrotron losses and particle escape, in the context of the leaky box model for particle acceleration by fluid shear and cosmic-ray viscosity.

5.1. Relativistic Transport Equations for Cosmic-Rays

Consider the relativistic transport equation for cosmic-rays, including telegrapher equation effects, for particle acceleration in a relativistic shear flow, which was discussed at the 2018 AGU meeting by Webb et al. (2018b).

The derivation of the diffusive transport Equation (1) is based on the first three moments of the relativistic Boltzmann equation (Webb 1989). By including cosmic-ray inertia terms in the analysis of the first and second moment equations implies that the diffusive transport Equation (1) can be generalized to the telegrapher transport equation (Webb et al. 2018b):

$$\begin{aligned}&\nabla_\alpha[cu^\alpha f_0 + q^\alpha] + \frac{1}{p^2}\frac{\partial}{\partial p}\\&\times\left[-\frac{p^3}{3}cu^\beta_{;\beta}f_0 - p^3\left(\frac{p^0}{p}\right)^2\dot{u}_\beta q^\beta - \Gamma\tau p^4\frac{\partial f_0}{\partial p}\right]\\&+\gamma^2\tau\frac{d^2 f_0}{dt^2} - \gamma\tau\frac{d}{dt}\left(\frac{p'}{3}c\nabla_\alpha u^\alpha\frac{\partial f_0}{\partial p}\right) = Q, \end{aligned}\tag{100}$$

where

$$\frac{d}{dt} = \frac{\partial}{\partial t} + \boldsymbol{u}\cdot\nabla \tag{101}$$

is the advective time derivative (Lagrangian time derivative) following the flow, and

$$q^\alpha = -\kappa^{\alpha\beta}\left[\nabla_\beta f_0 - \dot{u}_\beta\frac{(p^0)^2}{p}\frac{\partial f_0}{\partial p}\right] \tag{102}$$

is the relativistic diffusive flux of particles, and $\kappa^{\alpha\beta}$ is the diffusion tensor.

An alternative form of Equation (100) that has a more covariant form is

$$\begin{aligned}&\nabla_\alpha[cu^\alpha f_0 + q^\alpha] + \frac{1}{p^2}\frac{\partial}{\partial p}\\&\times\left[-\frac{p^3}{3}cu^\beta_{;\beta}f_0 - p^3\left(\frac{p^0}{p}\right)^2\dot{u}_\beta q^\beta - \Gamma\tau p^4\frac{\partial f_0}{\partial p}\right]\\&+c\tau u^\beta\nabla_\beta\left\{\nabla_\alpha(cu^\alpha f_0') - \frac{1}{p'^2}\frac{\partial}{\partial p'}\right.\\&\left.\times\left[\frac{p'^3}{3}c\nabla_\alpha u^\alpha f_0'\right]\right\} = Q. \end{aligned}\tag{103}$$

The derivation of Equations (100) or (103) is an approximation, which depends on the ordering of the different terms in the moment equations.

For the case of particle acceleration in a cylindrically symmetric shear flow about the axis of the jet, the transport Equations (100) or (103) reduce to the equation

$$\begin{aligned}&\tilde{\gamma}^2\tau\frac{\partial^2 f_0}{\partial t^2} + \gamma\frac{\partial f_0}{\partial t} - \frac{1}{r}\frac{\partial}{\partial r}\left(r\kappa\frac{\partial f_0}{\partial r}\right)\\&-\frac{1}{p^2}\frac{\partial}{\partial p}\left(\Gamma p^4\tau\frac{\partial f_0}{\partial p}\right) - \frac{1}{p^2}\frac{\partial}{\partial p}(D_s p^4 f_0) = Q, \end{aligned}\tag{104}$$

where $\tilde{\gamma}^2 = \gamma^2(1 - \beta^2/3)$, and γ is the relativistic γ of the flow. In Equation (104), we have included the effects of synchrotron losses, which are not present in Equations (100)–(103).

If one uses a leaky box model for the spatial diffusive transport term in Equation (104) in which the spatial diffusion term is replaced by $f_0/\tau_{\rm esc}$ where $\tau_{\rm esc}(p)$ is the escape time from the box, then the resultant transport equation resembles a wave equation in t, and $\zeta = \ln(p/p_0)$ for the highest derivative terms. The resultant leaky box equation has characteristic manifold $\phi(t, p) = $ const. that corresponds to the wave front in (t, ζ)-space, where ϕ satisfies the first-order partial differential equation

$$G \equiv \tau[\tilde{\gamma}^2\phi_t^2 - \Gamma\phi_\zeta^2] = 0 \quad \text{where} \quad \zeta = \ln(p/p_0) \tag{105}$$

(Webb et al. 2018a, Appendix E; Webb et al. 2019, Appendix D; Sneddon 1957). The Cauchy characteristics of Equation (105) (i.e., the bi-characteristics of the corresponding telegrapher equation for f_0), are

$$\frac{dp}{dt} = \pm\frac{\sqrt{\Gamma}p}{\tilde{\gamma}}, \tag{106}$$

(Webb et al. 2018a, 2019). Taking the positive sign characteristic in Equation (106) and integrating Equation (106) gives the formula

$$p = p_{\max}(t) = p_0 \exp\left(\frac{\sqrt{\Gamma}\, t}{\tilde{\gamma}}\right), \tag{107}$$

for the maximum particle momentum for the leaky box, telegrapher equation model. The result of Equation (107) can be written in the form

$$t(p, p_0) = \frac{\tilde{\gamma}}{\sqrt{\Gamma}} \ln\left(\frac{p}{p_0}\right), \tag{108}$$

which gives the minimum time for particles to be accelerated from momentum $p = p_0$ up to momentum p. In the above analysis, we have assumed that Γ and $\tilde{\gamma}$ are constants.

More generally, one can determine the characteristic manifold $\phi(t, p, r) = \text{const.}$ that represents the leading wave front for the spatial diffusive telegrapher Equation (104). The bi-characteristic equation solutions in that case are described in Webb et al. (2018a), Appendix E. In the Section 5.2, we look at the mean momentum $\langle p(t)\rangle$ obtained from an analysis of the Berezhko (1982) shear acceleration Green's function. It gives the unphysical result that the particles can gain an infinite momentum in a finite time. This is due to the neglect of the $f_{0,\mathrm{tt}}$ term in the telegrapher transport equation, which takes into account the finite cosmic-ray inertia.

5.2. The Berezhko (1982) Green's Function

Berezhko (1982) and Rieger & Duffy (2006) derived a Green's function solution for particle acceleration in a shear flow due to cosmic-ray viscosity. They solved the time-dependent version of the transport Equation (104) for the Green's function solution of the equation

$$\gamma\frac{\partial f_0}{\partial t} - \frac{1}{p^2}\frac{\partial}{\partial p}\left(\Gamma p^4 \tau \frac{\partial f_0}{\partial p}\right) = Q\delta(p - p_0)\delta(t), \tag{109}$$

for the case of nonrelativistic flows ($\gamma \to 1$). The scattering time $\tau(p)$ was of the form

$$\tau = \tau_0 \bar{p}^{\alpha}, \quad \bar{p} = \frac{p}{p_0}. \tag{110}$$

For the sake of simplicity, they neglected the diffusive and convective transport and took the shear acceleration coefficient Γ as constant. They considered the case of nonrelativistic flows for which $\gamma \to 1$. However, their solution also applies for relativistic flows if one notes that $t_m = t/\gamma$ is the time in the frame moving with the flow. In Equation (109), γ is the relativistic gamma of the flow (assumed to be constant).

As already pointed out in Equation (59), Equation (109) can be written in the form

$$\gamma\frac{\partial f_0}{\partial t} + \frac{1}{p^2}\frac{\partial}{\partial p}\left(\left\langle\frac{\Delta p}{\Delta t}\right\rangle p^2 f_0\right) - \frac{1}{p^2}\frac{\partial^2}{\partial p^2}\left(\left\langle\frac{(\Delta p)^2}{2\Delta t}\right\rangle p^2 f_0\right) = Q_0\delta(p - p_0)\delta(t) \tag{111}$$

where

$$\left\langle\frac{\Delta p}{\Delta t}\right\rangle = \frac{1}{p^2}\frac{\partial}{\partial p}(\Gamma p^4 \tau), \quad \left\langle\frac{(\Delta p)^2}{2\Delta t}\right\rangle = \Gamma p^2 \tau. \tag{112}$$

From Equation (112), one obtains an instantaneous momentum drift acceleration timescale

$$t_{\mathrm{acc}}^{(m)} = \frac{p}{\langle\Delta p/\Delta t\rangle} = \frac{1}{(4 + \alpha)\Gamma\tau}, \tag{113}$$

where we assume $\tau = \tau_0 (p/p_0)^{\alpha}$.

However, there is another method that can be used to extract an acceleration timescale $\langle t(p)\rangle$ for the acceleration (deceleration) of particles with momentum $p = p_0$ at time $t = 0$ up to momentum p, which can be derived using the Berezhko (1982) Green's function solution of Equation (109). The Berezhko (1982) Green's function can be written in the form

$$f_0(p, t) = \frac{Q_0}{\alpha\Gamma\tau_0 p_0 t}\bar{p}^{-(3+\alpha)/2} \exp\left[-\frac{(1 + \bar{p}^{-\alpha})}{\alpha^2\Gamma\tau_0 t}\right] I_{\nu} \times \left[\frac{2}{\alpha^2\Gamma\tau_0 t}(\bar{p})^{-(\alpha/2)}\right], \tag{114}$$

where $\nu = |1 + 3/\alpha|$. Here, we identify $t \equiv t^{(m)}$ with the time as measured in the co-moving frame. The time $t^{(I)} = \gamma t^{(m)}$ is the time in the fixed inertial frame (i.e., one can easily transform the time between frames). The mean acceleration time $\langle t(p)\rangle$ for the Green's function in Equation (114) is formally defined by the equation

$$\langle t(p)\rangle = \int_0^{\infty} t f_0(p, t)\, dt \Big/ \int_0^{\infty} f_0(p, t)\, dt, \tag{115}$$

where $f_0(p, t)$ is given by Equation (114).

Straightforward evaluation of the integrals in Equation (115) gives

$$n(p) = \int_0^{\infty} f_0(p, t)\, dt = \frac{A}{\nu}(\bar{p})^{-a}[(\bar{p})^{-a} H(p - p_0) + \bar{p}^{a} H(p_0 - p)], \tag{116}$$

where

$$A = \frac{Q_0}{|\alpha|\Gamma p_0 \tau_0}, \quad a = \frac{3 + \alpha}{2}. \tag{117}$$

(see Appendix C). A similar calculation gives

$$n(p)\langle t(p)\rangle \equiv \int_0^{\infty} t f_0(p, t)\, dt = A(\bar{p})^{-a}\Gamma(\nu - 1)\frac{|1 - (\bar{p})^{-\alpha}|}{\alpha^2\Gamma\tau_0} P_{-2}^{-\nu}\left(\frac{1 + (\bar{p})^{-\alpha}}{|1 - (\bar{p})^{-\alpha}|}\right), \tag{118}$$

where $P_{\mu}^{\nu}(z)$ is the standard associated Legendre function (e.g., Erdelyi et al. 1954, Vol. 1, Appendix, p. 370: see also Abramowitz & Stegun 1965, Ch. 8. p. 332 et seq.). The detailed derivation of Equation (118) is given in Appendix C.

Using Equations (116) and (118), we obtain

$$\langle t(p)\rangle = \frac{\nu\Gamma(\nu-1)}{\alpha^2\Gamma\tau_0}\Bigg\{\bar{p}^a(1-(\bar{p})^{-\alpha}) \times P_{-2}^{-\nu}\left(\frac{1+(\bar{p})^{-\alpha}}{1-(\bar{p})^{-\alpha}}\right)H(p-p_0) + \bar{p}^{-a}((\bar{p})^{-\alpha}-1)P_{-2}^{-\nu} \times \left(\frac{(\bar{p})^{-\alpha}+1}{(\bar{p})^{-\alpha}-1}\right)H(p_0-p)\Bigg\}. \quad (119)$$

The function $P_\nu^\mu(x)$ is given by

$$P_\nu^\mu(z) = \frac{1}{\Gamma(1-\mu)}\left(\frac{z+1}{z-1}\right)^{\mu/2} \times {}_2F_1\left(-\nu, \nu+1; 1-\mu; \frac{1}{2}(1-z)\right), \quad (120)$$

(Erdelyi et al. 1954, Vol. 1, Appendix, p. 370), where ${}_2F_1(a, b; c; z)$ is Gauss's hypergeometric function (see also Abramowitz & Stegun 1965, p. 332, formula 8.1.2). Using Equation (120), we obtain

$$P_{-2}^{-\nu}(\Omega) = \frac{1}{\Gamma(\nu+1)}\left(\frac{\Omega+1}{\Omega-1}\right)^{-\nu/2}\left[1+\frac{(\Omega-1)}{\nu+1}\right], \quad (121)$$

for the $P_{-2}^{-\nu}(\Omega)$ term in Equation (119).

Equations (119)–(121) give

$$\langle t(p)\rangle = \frac{1}{\alpha^2\Gamma\tau_0}\frac{1}{(\nu-1)} \times \left\{\left[1-(\bar{p})^{-\alpha}+\frac{2}{\nu+1}(\bar{p})^{-\alpha}\right]H(p-p_0) + \left((\bar{p})^{-\alpha}-1+\frac{2}{\nu+1}\right)H(p_0-p)\right\}. \quad (122)$$

For $p > p_0$, Equation(122) may be inverted to give the equation

$$\bar{p} = \left\{\frac{\nu+1}{\nu-1}[1-3\alpha\Gamma\tau_0\langle t(p)\rangle]\right\}^{-1/\alpha}, \quad (123)$$

which implies that

$$p \to \infty \quad \text{as} \quad \langle t\rangle \to (3\alpha\Gamma\tau_0)^{-1}, \quad (124)$$

which seems to suggest that particles can be accelerated to an infinite momentum in a finite time. This unphysical, noncausal behavior was also noted by Webb et al. (2019) based on integrating Equation (113) with respect to p. Webb et al. (2019) argued that this noncausal behavior of the Fokker Planck Equation (109) could be corrected in part by including a second-order time derivative term in Equation (109) representing the cosmic-ray inertia.

The acceleration timescale $pd\langle t\rangle/dp$ for $p > p_0$ deduced from Equation (122) is

$$p\frac{d\langle t(p)\rangle}{dp} = \frac{1}{(2\alpha+3)\Gamma\tau}. \quad (125)$$

Comparing Equation (113) with Equation (125), we obtain

$$\frac{pd\langle t(p)\rangle/dp}{t_{\rm acc}^{(m)}} = \frac{4+\alpha}{2\alpha+3}. \quad (126)$$

Thus, the two timescales $pd\langle t(p)\rangle/dp$ and $t_{\rm acc}^{(m)}$ are of approximately the same value for $0 < \alpha < 1$ (the ratio (126) is unity for $\alpha = 1$).

The timescale $\langle t(p)\rangle$ in Equation (122) gives the mean time for particles to be accelerated from momentum $p = p_0$ up to momentum p. This timescale is clearly different from the timescale $t_{\rm acc}^{(m)}$ in Equation (113). Note that $t_{\rm acc}^{(m)}$ is an instantaneous timescale representing the mean drift in the particle momentum as occurs, for example, in a stochastic differential equation formulation of the Fokker Planck equation (i.e., it does not represent a global timescale). The acceleration time $\langle t(p)\rangle$ is an average over all possible times weighted by the Green's function in Equation (114). The mean timescale for acceleration $\langle t(p)\rangle$ is analogous to the acceleration timescale for particles to be accelerated from momentum $p = p_0$ up to momentum p in the theory of DSA by the first-order Fermi mechanism at astrophysical shocks as obtained by Axford (1981) and Drury (1983). Also note that $\langle t(p)\rangle$ applies to decelerated particles with $p < p_0$ in Equation (119).

5.3. Leaky Box Models of Particle Acceleration

The leaky box model of particle acceleration due to cosmic-ray viscosity in radio-jet shear flows developed by Rieger & Duffy (2019) can be modified to include synchrotron losses of electrons at TeV energies (and above) and also for protons at EeV energies. The basic leaky box model in Equation (56) modified to take into account synchrotron losses and inverse Compton losses has the form

$$-\frac{1}{p^2}\frac{\partial}{\partial p}\left(\Gamma p^4\tau\frac{\partial f_0}{\partial p}\right) - \frac{1}{p^2}\frac{\partial}{\partial p}(D_s p^4 f_0) + \frac{f_0}{t_{\rm esc}} = Q. \quad (127)$$

The basic leaky box Equation (127) can be derived by using the steady-state version of the relativistic diffusive transport Equation (104), including the effects of synchrotron losses (Webb et al. 1984), in which the first and second time derivatives are set equal to zero. The spatial diffusion term is replaced by $-f_0/t_{\rm esc}$ representing particle escape from the leaky box.

The timescales of the different terms in the leaky box model in Equation (127) refer to timescales in the co-moving plasma frame, and this should be kept in mind in the analysis below. The timescale Δt^I in the fixed inertial frame is related to the corresponding timescale $\Delta t^{(m)}$ in the flow frame by the Lorentz transformation

$$(\Delta t)^I = \gamma(\Delta t)^{(m)}. \quad (128)$$

In this section, we will use timescales as calculated in the moving frame (i.e., in the fluid frame). It is straightforward in principle to transform to timescales to the fixed frame.

A version of this leaky box model is described in Webb et al. (2019, their Appendix E), where the case $t_{\rm esc} \to \infty$ was studied in detail. Following the analysis of Section 3, we take the escape time $t_{\rm esc}$, in the region $0 < r < r_2$ to be related to the diffusion $\kappa_\perp = (\Delta r)^2/2\Delta t$, which gives the escape time estimate

$$t_{\rm esc}=t_{\rm esc}^0\left(\frac{p}{p_0}\right)^{-\alpha},\quad t_{\rm esc}^0=\frac{3}{2}\left(\frac{r_2^2}{c^2}\right)\frac{1}{\tau_0}. \tag{129}$$

For synchrotron losses:

$$\left\langle\frac{dp}{dt}\right\rangle=-\frac{p}{t_{\rm sync}}=-D_s p^2, \tag{130}$$

where

$$D_s=\frac{1}{m_0 c\tau_r},\quad \tau_r=\frac{6\pi m_0 c}{\sigma_{\rm T}B^2},$$
$$\sigma_{\rm T}=\frac{8\pi r_0^2}{3},\quad r_0=\frac{e^2}{m_0c^2},\quad t_{\rm sync}=\frac{\tau_r}{\gamma_p\beta_p}. \tag{131}$$

Here, m_0 denotes the particle rest mass and $\gamma_p=(1-\beta_p^2)^{-1/2}$ is the particle Lorentz factor; $\beta_p=v/c$; $\sigma_{\rm T}$ is the Thomson cross-section ($m_0=m_e$ for electrons and $m_0=m_p$ for protons). Formulas in Equation(130)–(131) are in cgs units.

Using the normalized particle momentum $\bar{p}=p/p_0$, the leaky box Equation (127) reduces to the ordinary differential equation

$$\frac{d^2f_0}{d\bar{p}^2}+\frac{df_0}{d\bar{p}}\left[\frac{4+\alpha}{\bar{p}}+\chi(\bar{p})^{-\alpha}\right]+f_0[4\chi(\bar{p})^{-\alpha-1}-\delta(\bar{p})^{-2}]=-\frac{Q}{\Gamma\tau_0\bar{p}^{\alpha+2}} \tag{132}$$

where

$$\chi=\frac{D_s p_0}{\Gamma\tau_0},\quad \delta=\frac{1}{\Gamma\tau_0 t_{\rm esc}^0}. \tag{133}$$

The dimensionless parameters χ and δ are given by the formulae

$$\chi=(4+\alpha)\frac{t_{\rm acc}}{t_{\rm sync}},\quad \delta=(4+\alpha)\frac{t_{\rm acc}}{t_{\rm esc}}, \tag{134}$$

where

$$t_{\rm acc}=\frac{1}{(4+\alpha)\Gamma\tau_0}(\bar{p})^{-\alpha},\quad t_{\rm esc}=t_{\rm esc}^0(\bar{p})^{-\alpha},$$
$$t_{\rm sync}=\frac{1}{D_s p_0}(\bar{p})^{-1}. \tag{135}$$

Equation (132) in general can be integrated (either numerically or analytically).

5.3.1. The $\alpha=1$ Case

Below, we consider the special case $\alpha=1$ and later the cases $0<\alpha<1$ and $\alpha>1$ separately. The case $\alpha=1$ corresponds to Bohm diffusion, and we set the source term $Q=0$ since we are interested mainly in the balances between particle acceleration, synchrotron losses, and particle escape in shaping the particle momentum spectrum. For the case $\alpha=1$, Equation (132) reduces to the equation

$$\frac{d^2f_0}{d\bar{p}^2}+\frac{1}{\bar{p}}\frac{df_0}{d\bar{p}}[4+\alpha+\chi]+\frac{f_0}{\bar{p}^2}[4\chi-\delta]=0. \tag{136}$$

Searching for a solution of Equation (136) for $f_0\propto p^{-\mu}$, we obtain the quadratic equation

$$\mu^2-\mu(4+\chi)+(4\chi-\delta)=0, \tag{137}$$

for the spectral exponent μ.

The roots $\mu_\pm$ of the quadratic Equation (137) are given by the quadratic formula

$$\mu_\pm=\frac{1}{2}\{4+\chi\pm[(4+\chi)^2-4(4\chi-\delta)]^{1/2}\}$$
$$\equiv(2+\chi/2)\pm[(2-\chi/2)^2+\delta]^{1/2}. \tag{138}$$

Standard results for the roots of a quadratic equation give

$$\mu_+\mu_-=4\chi-\delta,\quad \mu_++\mu_-=4+\chi. \tag{139}$$

There are three cases to consider:

Case (i) $(4\chi-\delta)<0$.

Using Equations (134) and (135), we find

$$4\chi-\delta=\delta\left(\frac{4t_{\rm esc}}{t_{\rm synch}}-1\right)<0\quad\text{if}\quad\frac{t_{\rm esc}}{t_{\rm synch}}<\frac{1}{4}, \tag{140}$$

which means that the escape time is less than one quarter of the synchrotron loss time.

In this case, $\mu_+\,\mu_-<0$ and only the positive root μ_+ is applicable to describe the spectrum $f_0\propto p^{-\mu_\infty}$ where

$$\mu_\infty=\mu_+=(2+\chi/2)+[(2-\chi/2)^2+\delta]^{1/2}. \tag{141}$$

Note that this case includes the case of no losses with $\chi=0$, which corresponds to the Green's function solution and monoenergetic spectrum solutions of Sections 3 and 4 for the case $\alpha=1$. Note $\mu_\infty=\mu_+$ and that the root $\mu=\mu_-$ presumably applies at smaller momentum.

Case (ii) $(4\chi-\delta)=0$.

In this case, the roots of the quadratic Equation (137) for μ are

$$\mu=0,\quad \mu\equiv\mu_\infty=4+\chi. \tag{142}$$

Clearly, $\mu_\infty=4+\chi$ in this case, and the $\mu=0$ root corresponds to the spectrum at low momenta (however, the model only applies to relativistic particles).

Case (iii) $(4\chi-\delta)>0$.

This is the case of strong synchrotron losses compared to the effects of particle escape. Both μ_+ and μ_- are positive. The general solution of the homogeneous differential Equation (136) is of the form

$$f_0=a_1(\bar{p})^{-\mu_-}+a_2(\bar{p})^{-\mu_+}, \tag{143}$$

where a_1 and a_2 are arbitrary constants. As $p\to\infty$, the spectrum is dominated by the softest power law in (143), i.e., $f_0\propto p^{-\mu_\infty}$ where

$$\mu_\infty=\mu_+=(2+\chi/2)+[(2-\chi/2)^2+\delta]^{1/2}. \tag{144}$$

Synchrotron losses dominate the particle escape in determining the spectrum. In the limit of no particle escape ($\delta\to0$ and $\tau_{\rm esc}^0\to\infty$), Equation (144) gives

$$\mu_\infty=\begin{cases}4 & \text{if}\quad \chi<4,\\ \chi & \text{if}\quad \chi>4.\end{cases} \tag{145}$$

Thus, $\mu_\infty=\max(\chi,4)$. Notice that the μ_+ root is continuous as χ increases through $\chi=\delta/4$. The μ_- root in all cases represents the low momentum part of the spectrum, and μ_+ represents the high momentum end of the spectrum. The spectrum is convex in all cases (i) $4\chi - \delta < 0$, (ii) $4\chi - \delta = 0$, and (iii) $4\chi - \delta > 0$. In case (iii), there is a strong fall off (steep spectrum) due to the dominant synchrotron losses. We do not expect the spectrum to suddenly flip from convex to concave as one passes through the different regimes and transition point (i)–(iii) as χ increases.

Case $\tau_{\rm esc} \propto \bar{p}^{-\nu}$ where $\nu = \alpha + 2$.

Other functional forms for $\bar{f}(\bar{p})$ are obtained as $\bar{p} \to \infty$ for different choices of $\tau_{\rm esc}(\bar{p})$. For example, for the case

$$\tau_{\rm esc}(\bar{p}) = \tau_{\rm esc}^0 (\bar{p})^{-\nu}, \tag{146}$$

with

$$\alpha = 1, \quad \nu = 2 + \alpha = 3, \tag{147}$$

so that $\delta(\bar{p})^{-2} \to \delta(\bar{p})^{(\nu-2-\alpha)}$ in Equation (132), then the modified, homogeneous Equation (132) has solutions

$$\bar{f}_0 = (\bar{p})^{-(\chi+4)/2}\{a_1 I_{|(4-\chi)/2)|}(\sqrt{\delta}\bar{p}) + a_2 K_{|(4-\chi)/2|}(\sqrt{\delta}\bar{p})\}, \tag{148}$$

where $I_m(z)$ and $K_m(z)$ are modified Bessel functions of the first and second kind. Choosing $a_1 = 0$ (so that $f_0 \to 0$ as $\bar{p} \to \infty$), one then obtains

$$\bar{f}_0 \sim a_2(\bar{p})^{-(\chi+5)/2} \exp(-\sqrt{\delta}\bar{p}) \quad \text{as} \quad \bar{p} \to \infty. \tag{149}$$

In this case, $\bar{f}_0$ has the form of a power law times an exponential fall off as $\bar{p} \to \infty$ (i.e., $\bar{f}_0$ does not need to be a power-law fall off as $\bar{p} \to \infty$).

Case: $\tau \propto \bar{p}^{\alpha}$, $\tau_{\rm esc} \propto \bar{p}^{-\alpha}$, $4\chi < \delta$ (weak synchrotron losses).

For $4\chi < \delta$ (weak synchrotron losses), we obtain

$$\mu_\infty = (a + \chi/2) + [(a + \chi/2)^2 + \delta - 4\chi]^{1/2}, \tag{150}$$

as the asymptotic spectral index of particles at large momenta ($p \gg p_0$), where $a = (3 + \alpha)/2$ as in (64) and $\alpha = 1$.

The formula of Equation (150) for μ_∞ can be written in terms of the ratios $t_{\rm acc}/t_{\rm esc}$ and $t_{\rm acc}/t_{\rm sync}$ where $t_{\rm acc}$, $t_{\rm esc}$, and $t_{\rm sync}$ are the characteristic acceleration time, escape time, and synchrotron loss time, respectively, using Equations (134) and (135).

In the limit as $\chi \to 0$ ($t_{\rm sync} \to \infty$), the formulas in Equations (150) and (134) gives

$$\mu_\infty = a + [a^2 + (4 + \alpha)t_{\rm acc}/t_{\rm esc}]^{1/2}, \tag{151}$$

which is the Equation (64) that was originally derived by Rieger & Duffy (2019) for shear acceleration in the absence of synchrotron losses. This formula holds for $\alpha \neq 1$ as well as for $\alpha = 1$. The formula encapsulates the formulas for μ_∞ in Equations (70)–(72), which take into account the complicated dependence of μ_∞ on β_0, β_2, and the scattering confinement parameter ϵ that describes the effect of particle scattering outside the jet (i.e., in $r > r_2$). Formula (150) generalizes the formula (151) to take into account synchrotron losses for the case $\alpha = 1$.

5.3.2. The $0 < \alpha < 1$ Case

For the $\alpha < 1$ case, we search for solutions of the leaky box Equation (132) with leading order term $f_0 \propto p^{-\mu}$. Note that this analysis implies that there is a power-law dependence of f_0 on p as $p \to \infty$, which in turn may possibly be multiplied by an exponential fall off with p as $p \to \infty$. A more detailed analysis is needed to investigate the problem. The largest terms in the balance of powers in Equation (132) in this case require

$$p^{-\mu-1-\alpha}\chi(-\mu + 4) = 0, \quad \text{with solution} \quad \mu = 4. \tag{152}$$

5.3.3. The $\alpha > 1$ Case

Similarly, for the case $\alpha > 1$, we we seek solutions with $f_0 \propto p^{-\mu}$ as $p \to \infty$ (as in $0 < \alpha < 1$ analysis, there may also be an exponential fall-off term modifying the power-law fall off for large p). The largest terms are proportional to $p^{-\mu-2}$, and balance of these terms in Equation (132) with $Q = 0$, gives the equation:

$$\mu^2 - (3 + \alpha)\mu - \delta = 0, \tag{153}$$

with solution:

$$\begin{aligned}\mu \equiv \mu_\infty &= a + [a^2 + \delta]^{1/2}\\ &\equiv a + [a^2 + (4 + \alpha)t_{\rm acc}/t_{\rm esc}]^{1/2},\end{aligned} \tag{154}$$

which is equivalent to the formula in Equations (65) or (151) for μ_∞ that is obtained in the case of no synchrotron losses.

5.4. Timescale Estimates and μ_∞ Estimates

A naive approach to the evaluation of $t_{\rm esc}$ based on Equation (135) needs to be modified to take into account that $t_{\rm esc}^0$ and τ_0 should depend on the effects of scattering outside the jet in $r > r_2$. The ratio of $t_{\rm acc}/t_{\rm esc}$ in Equation (72) does not need to be modified since it takes into account scattering in both $0 < r < r_2$ and in $r > r_2$. We take the formula in Equation (72) to be applicable in its present form. The escape time $t_{\rm esc}$, and the acceleration time $t_{\rm acc}$ in principle should depend on the scattering in both $0 < r < r_2$ and in $r > r_2$.

Based on these heuristic considerations, we suggest that the acceleration time formula $t_{\rm acc}$ should be modified to the form

$$\begin{aligned}t_{\rm acc} &= \frac{1}{(4+\alpha)\Gamma}\left(\frac{1}{\tau_1} + \langle\nu(r_2, p; R)\rangle\right)\\ &\to \frac{15}{(4+\alpha)}\frac{1}{\eta_2^2}\frac{r_2^2}{c^2\tau_0}\\ &\quad\times\left(1 + \frac{1}{s}\right)(\bar{p})^{-\alpha} \text{ as as } R \to \infty\end{aligned} \tag{155}$$

where we have used Equations (76)–(78) for $\langle\nu(r_2, p; R)\rangle$, and $\tau_1 = \tau_0\bar{p}^{\alpha}$ is the scattering time in the region $0 < r < r_2$. This formula for $t_{\rm acc}$ differs from the formula for $t_{\rm acc}$ in Equation (135) by the extra factor of $(1 + 1/s)$. Using Equation (155) for $t_{\rm acc}$ and Equation (72) for $t_{\rm acc}/t_{\rm esc}$, we obtain the modified formula for $t_{\rm esc}$ (in the case $R \to \infty$) as

$$t_{\rm esc} = \frac{3}{j_1(\epsilon)^2}\frac{r_2^2}{c^2\tau_0}\left(1 + \frac{1}{s}\right)(\bar{p})^{-\alpha}. \tag{156}$$

The modified Equation (155) and (156) take into account the heuristic physical arguments given above.

Notice that in the case of free escape of particles from the region $0 < r < r_2$, $s \to \infty$, and the timescale $t_{\rm acc}$ does not depend on the scattering in $r > r_2$. In the limit of very small s ($s \neq 0$), the boundary condition at $r = r_2$, (31) becomes a Von

Neumann boundary condition. In this case, all particles that attempt to cross the boundary at $r = r_2$ are reflected back into the region $0 < r < r_2$. In this limit, the mean scattering frequency is dominated by the scattering in $r > r_2$. Put another way

$$\nu_{12} = \nu_1 + \nu_2, \quad \frac{1}{\tau_{12}} = \frac{1}{\tau_1} + \frac{1}{\tau_2} \quad \text{or} \quad \tau_{12} = \frac{\tau_1\tau_2}{\tau_1 + \tau_2}, \tag{157}$$

where $\nu_1 = 1/\tau_1$ and $\nu_2 = 1/\tau_2$. Thus, the mean scattering time τ_{12} is half the harmonic mean of τ_1 and τ_2 where τ_1 is the mean scattering time in $0 < r < r_2$ and τ_2 is the mean scattering time in $r > r_2$. The harmonic mean $H(\tau_1, \tau_2) = 2\tau_1\tau_2/(\tau_1 + \tau_2)$. The same rule describes the effective resistance R of two resistors R_1 and R_2 in parallel in an electronic circuit, i.e., $R = R_1R_2/(R_1 + R_2)$.

However, a more exact analysis may well differ in the details for the estimation of the timescales $t_{\rm acc}$ and $t_{\rm esc}$. Notice that the escape time $t_{\rm esc} \to \infty$ as $\epsilon \to \infty$ because $j_1(\epsilon) \to 0$ as $\epsilon \to \infty$. This effectively means that the particles are strongly confined to the vicinity of the jet for strong scattering in the region $r > r_2$ in the limit as $\epsilon \to \infty$.

The other timescale of interest in applications is the synchrotron loss timescales $t^{(e)}_{\rm synch}$ and $t^{(p)}_{\rm synch}$ for protons. The synchrotron loss timescale for species α is given by

$$t^{(\alpha)}_{\rm synch} = \frac{\tau_{r\alpha}}{\gamma_\alpha}, \quad \alpha = p, e. \tag{158}$$

Straightforward calculations using Equation (129)–(130) give the formulae

$$\begin{aligned} \tau_{rp} &= \frac{6\pi m_p c}{\sigma_{Tp} B^2} = 4.79 \times 10^{28}\left(\frac{B}{10\ \mu\mathrm{G}}\right)^{-2}\ \mathrm{s} \\ \tau_{re} &= \frac{\tau_{rp}}{1836^3} = 1.6158 \times 10^{-10}\tau_{rp}. \end{aligned} \tag{159}$$

Thus,

$$\begin{aligned} \tau_{rp} &= 4.79 \times 10^{28}\left(\frac{B}{10\ \mu\mathrm{G}}\right)^{-2}\ \mathrm{s}, \\ \tau_{re} &= 7.743 \times 10^{18}\left(\frac{B}{10\ \mu\mathrm{G}}\right)^{-2}\ \mathrm{s}. \end{aligned} \tag{160}$$

Then, using Equation (131) and setting $\beta_p \sim 1$ and $\beta_e \sim 1$, we obtain the formulae

$$\begin{aligned} t^{(p)}_{\rm synch} &= 4.794 \times 10^{19}\left(\frac{B}{10\ \mu\mathrm{G}}\right)^{-2}\left(\frac{\gamma_p}{10^9}\right)^{-1}\ \mathrm{s}, \\ t^{(e)}_{\rm synch} &= 7.743 \times 10^{9}\left(\frac{B}{10\ \mu\mathrm{G}}\right)^{-2}\left(\frac{\gamma_e}{10^9}\right)^{-1}\ \mathrm{s}, \end{aligned} \tag{161}$$

for the synchrotron loss timescales for the protons and the electrons. The synchrotron loss timescales in Equation (161) can also be written as

$$\begin{aligned} t^{(p)}_{\rm synch} &= 1.426 \times 10^{12}\left(\frac{B}{10\ \mu\mathrm{G}}\right)^{-2}\left(\frac{E_p}{10^{18}\ \mathrm{eV}}\right)^{-1}\ \mathrm{yr}, \\ t^{(e)}_{\rm synch} &= 1.255 \times 10^{-1}\left(\frac{B}{10\ \mu\mathrm{G}}\right)^{-2}\left(\frac{E_e}{10^{18}\ \mathrm{eV}}\right)^{-1}\ \mathrm{yr}. \end{aligned} \tag{162}$$

Next, consider Equation (155) for $t_{\rm acc}$. It can be written in the form

$$t_{\rm acc} = \frac{5}{4 + \alpha}\frac{r_2^2}{\eta_2^2\kappa(p)}\left(1 + \frac{1}{s}\right), \tag{163}$$

where $\kappa(p) = c^2\tau/3$ is the particle diffusion coefficient in the jet in the region $0 < r < r_2$. Thus, the acceleration time is of the order of r_2^2/κ and, hence, depends on the half-width of the jet r_2 and on the diffusion coefficient $\kappa(p)$, which in turn depends on the power spectrum of the turbulence scattering the particles. The acceleration time also depends on the parameter η_2. Note that η_2 increases as β_0 increases and, hence, the acceleration time decreases as the β_0 increases, (i.e., relativistic jets accelerate the particles on shorter timescales as β_0 increases). Also note the dependence of $t_{\rm acc}$ on the particle scattering parameter s in the region outside the jet. Recall $s = \partial \ln\kappa/\partial\ln r$ in $r > r_2$. As $s \to 0$, formula, Equation (163) implies that $t_{\rm acc} \to \infty$. The net upshot is that if there is strong scattering ($s \to 0$ in $r > r_2$), one obtains a very hard spectrum for the accelerated particles, but it takes a very long time $t_{\rm acc}$ for the particles to be accelerated to a particular momentum p. Note that $\epsilon = k/s \to \infty$ as $s \to 0$ in the plot for μ_∞ in Figure 3. In the opposite limit, as $s \to \infty$, $\epsilon = k/s \to 0$, the spectrum of accelerated particles is much softer, as the boundary $r = r_2$ is a free-escape boundary in this limit.

5.4.1. Bohm Diffusion Case ($\alpha = 1$)

For the case $\alpha = 1$ (i.e., for $\kappa \propto p$),

$$\kappa(p) = \frac{v r_g}{3P_0}, \quad P_0 = \left(\frac{\delta B}{B}\right)^2, \quad v \sim c. \tag{164}$$

It is useful to note the formulae

$$\begin{aligned} r^{(p)}_g &= 3.1266 \times 10^{20}\left(\frac{\gamma_p}{10^9}\right)\left(\frac{B}{10\ \mu\mathrm{G}}\right)^{-1}\ \mathrm{cm}, \\ r^{(e)}_g &= 1.703 \times 10^{17}\left(\frac{\gamma_e}{10^9}\right)\left(\frac{B}{10\ \mu\mathrm{G}}\right)^{-1}\ \mathrm{cm}. \end{aligned} \tag{165}$$

Thus, for $\gamma_e = \gamma_p$, then $r^{(p)}_g/r^{(e)}_g = 1836$. Thus, protons and electrons with the same speed result in the electrons having a gyroradius of $1/1836$ that of the protons (note $m_p/m_e = 1836$ for rest mass ratio of the two species). However, if one uses the total energy of the particles, one obtains the formula

$$r_g = 3.333 \times 10^{20}\left(\frac{E}{10^{18}\ \mathrm{eV}}\right)\left(\frac{B}{10\ \mu\mathrm{G}}\right)^{-1}\ \mathrm{cm}, \tag{166}$$

for the gyroradius of the particles. This formula works for both the electrons and protons. These results are useful when evaluating the Bohm-like diffusion coefficient in Equation (164).

Equation (163) for t_{acc} for both protons and electrons reduces to the formula

$$t_{acc} = 9.058 \times 10^2 \left(\frac{P_0}{\eta_2^2}\right)\left(\frac{r_2}{100\ \mathrm{pc}}\right)^2\left(\frac{E}{10^{18}\ \mathrm{eV}}\right)^{-1} \times \left(\frac{B}{10\ \mu\mathrm{G}}\right)\left(1+\frac{1}{s}\right)\quad \mathrm{yr}. \tag{167}$$

The escape time t_{esc} for both protons and electrons is given by

$$t_{esc} = \frac{\eta_2^2}{j_1(\epsilon)^2} t_{acc}. \tag{168}$$

From Equations (162)–(168), we obtain

$$\frac{t_{acc}}{t_{esc}} = \frac{j_1(\epsilon)^2}{\eta_2^2}. \tag{169}$$

We also obtain the ratios

$$\frac{t_{acc}}{t_{\mathrm{sync}}^{(e)}} = 7.22 \times 10^3 \frac{P_0}{\eta_2^2}\left(\frac{r_2}{100\ \mathrm{pc}}\right)^2 \times \left(\frac{B}{10\ \mu\mathrm{G}}\right)^3\left(1+\frac{1}{s}\right),$$
$$\frac{t_{acc}}{t_{\mathrm{synch}}^{(p)}} = 6.35 \times 10^{-10} \frac{P_0}{\eta_2^2}\left(\frac{r_2}{100\ \mathrm{pc}}\right)^2 \times \left(\frac{B}{10\ \mu\mathrm{G}}\right)^3\left(1+\frac{1}{s}\right). \tag{170}$$

Note that $[t_{acc}/t_{\mathrm{synch}}^{(e)}]\big/[t_{acc}/t_{\mathrm{synch}}^{(p)}] = (m_p/m_e)^4$. Using Equations (168)–(170) in Equations (150)–(134) gives the formula for μ_∞ in the form

$$\mu_\infty = a + \frac{\chi}{2} + \left[\left(a+\frac{\chi}{2}\right)^2 + \delta - 4\chi\right]^{1/2},$$
$$\chi = 5\frac{t_{acc}}{t_{\mathrm{synch}}}, \qquad \delta = 5\frac{t_{acc}}{t_{esc}},$$
$$a = \frac{3+\alpha}{2} = 2, \qquad \alpha = 1. \tag{171}$$

From Equation (171), we obtain,

$$\mu_\infty = 2 + \frac{\chi}{2} + \left[\left(2-\frac{\chi}{2}\right)^2 + \delta\right]^{1/2}. \tag{172}$$

From Equation (172), one can show $d\mu_\infty/d\chi > 0$ for $\chi > 0$, i.e., the spectrum softens with increasing synchrotron losses. Equation (172) determines μ_∞ in terms of $t_{acc}/t_{\mathrm{synch}}$ and t_{acc}/t_{esc}, for the case where $\alpha = 1$ (Bohm diffusion case). For $\alpha < 1$, $\mu_\infty = 4$, and synchrotron losses dominate the spectrum. For $\alpha > 1$, μ_∞ is determined by α and by t_{acc}/t_{esc}.

From Equation (170), the acceleration time for protons is much less than the synchrotron loss timescale, and one can usually neglect the effect of synchrotron losses for protons. It is clear from Equation (170) that synchrotron losses are much more important for electrons. However, for nonrelativistic jets $\eta_2 \sim \beta_{02}$ as $\beta_{02} \to 0$. In this case, it is possible for the proton synchrotron loss time to become comparable to the acceleration time, but this corresponds to a nonrelativistic shear flow in which case the spectral index μ_∞ will be large, and the acceleration process will not be effective.

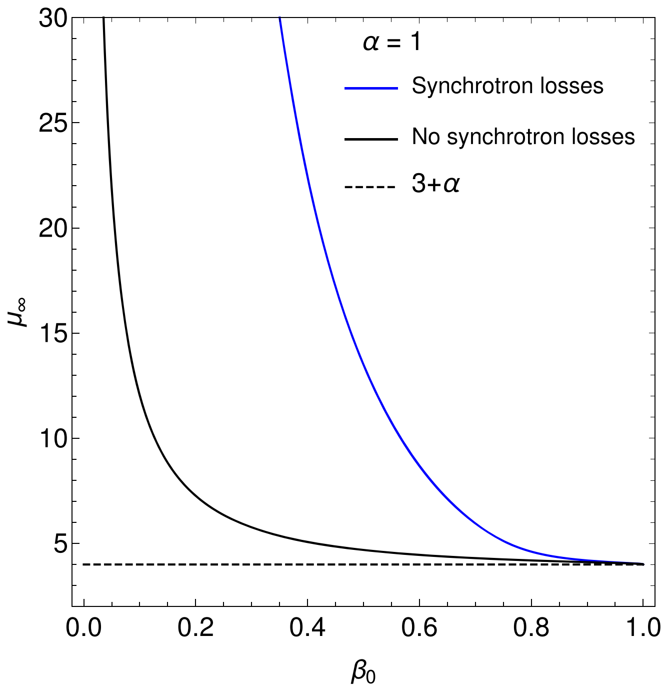

Figure 9. Plots of μ_∞ vs. the jet velocity β_0 from Equation (170)–(172), for the case of Bohm diffusion ($\alpha = 1$ and $\tau \propto p$) for electrons, for case (i) including synchrotron losses (blue curve) and for case (ii) with no synchrotron losses (black curve with $\chi = 0$). $\beta_2 = 0$, $s = 0.1$, $k = 1$, $\epsilon = k/s = 10$, $r_2/(100\ \mathrm{pc}) = 1$, $B/10\ \mu\mathrm{G} = 0.1$, and $P_0 = 0.01$.

Figure 9 shows plots of μ_∞ versus β_0 using Equations (170)–(172), which apply for the case of Bohm diffusion ($\alpha = 1$, $\tau \propto p$). The figure is for electrons with: $s = 0.1$, $k = 1$, i.e., $\epsilon = 10$, $r_2 = 100$ pc, $\alpha = 1$ so that $a = 2$. $P_0 = 0.01$ and $B/(10\ \mu\mathrm{G}) = 0.1$. The blue curve shows μ_∞ versus β_0 for the case including synchrotron losses and for the case of no synchrotron losses (the black curve). Clearly, the synchrotron losses lead to a softer spectrum (larger μ_∞) than the case without losses. Note that the the accelerated particles in the leaky box model should in general be constrained to have a gyroradius r_g that is less or much less than the width of the box. For the above parameters, the electron gyroradius of an $E = 10^{16}$ eV electron, from Equation (166) is $r_g \sim 3 \times 10^{19}$ cm, and the width of the jet $r_2 \sim 3 \times 10^{20}$ cm, i.e., $r_g/r_2 \sim 0.1$. However, the analysis cannot presumably be applied to $E_e = 10^{18}$ eV electrons because in that case, the gyroradius of the particles is greater than the width of the jet (i.e., $r_g \sim 3 \times 10^{21}$ cm in that case). However, the model includes particle scattering outside the width of the jet, so that restricting the particle gyroradius to be less than the width of the jet does not necessarily apply. Clearly, an acceleration model that includes the space variable r as an independent variable is important in such cases (i.e., a time and space dependent and momentum dependent solution of the problem may be necessary in conjunction with theory to resolve these problems). Much steeper spectra (larger μ_∞) for the synchrotron loss case are obtained for larger B.

It turns out (Section 5.3) that for the asymptotic momentum spectrum of the particles in the leaky box model for the case $0 < \alpha < 1$, synchrotron losses dominate shear acceleration and $f_0 \propto p^{-4}$ as $p \to \infty$. However for $\alpha > 1$, $f_0 \propto p^{-\mu_\infty}$ as $p \to \infty$ where μ_∞ is given by Equations (65) or (154), which corresponds to the case with no synchrotron losses. To get a better idea of the combined effect of synchrotron losses, particle energy gains due to shear acceleration, and the effects of particle scattering outside the shear flow, the spectrum should be investigated in more detail at lower and intermediate energies.

6. Conclusions

In this paper, we have re-visited the problem of particle acceleration by cosmic-ray viscosity in relativistic radio jets. In previous papers (Webb 1990; Webb et al. 2018a, 2019), we considered the case where particles freely escape from the shear flow region $0 < r < r_2$ after interacting with the flow. This case corresponds to imposing a Dirichlet boundary condition at the edge of the jet (either $f_0(r_2, p) = 0$ or $f_0(r_2, p)$ is specified at $r = r_2$) and that the diffusion coefficient $\kappa \to \infty$ in $r > r_2$.

It was pointed out by Webb et al. (2019) that more general boundary conditions can be imposed on the solutions in the form of a mixed Dirichlet–Von Neumann boundary condition at $r = r_2$ (see also Section 2.1 and Appendix B). This boundary condition allows for particle scattering in the outer region $r > r_2$ where we assume that there is no particle energization by shear acceleration, and the particle distribution function satisfies the cylindrical radial diffusion equation. The net effect of the particle scattering in $r > r_2$ results in a harder momentum spectrum of particles compared to the free-escape case. This is because particles exiting at $0 < r < r_2$ can now be scattered back into the shear flow region and can thus be further energized by the shear flow in $0 < r < r_2$.

Green's function solutions for the mixed, Dirichlet–Von Neumann boundary conditions at the edge of the jet at $r = r_2$ (Section 3) were used in conjunction with Green's formula to obtain solutions of boundary value problems in which the spectrum of particles, $f_0(\infty, p)$, is specified as $r \to \infty$. The Green's function solutions correspond to the case of steady-state injection of particles with momentum $p = p_0$ at radius $r = r_1$ inside the jet shear flow ($0 < r_1 < r_2$). Green's formula (Section 4) was used to obtain monoenergetic spectrum solutions with $f_0(\infty, p) = N_g \delta(p - p_0)/(4\pi p_0^2)$ as $r \to \infty$. The solutions in Sections 3 and 4, illustrate the hardening of the spectrum compared to the free-escape boundary condition solutions of Webb et al. (2018a, 2019), due to the effects of particle scattering outside the jet in the region $r > r_2$.

The asymptotic power-law spectral index of shear accelerated particles μ_∞ ($f_0 \propto p^{-\mu_\infty}$ as $p \to \infty$) is shown in Figure 3 as a function of the jet speed β_0 at $r = 0$ (we assumed that $\beta_2 = 0$ in Figure 3; more generally β_0 should be replaced by the relative velocity $\beta_{02} = (\beta_0 - \beta_2)/(1 - \beta_0\beta_2)$ if $\beta_2 \neq 0$). The effect of particle scattering outside the shear flow region $0 < r < r_2$ is parameterized by a single parameter $\epsilon = k/s$ where k characterizes the fluid velocity profile and gradient in $0 < r < r_2$ and $s = \partial \ln \tau / \partial \ln r$ where $\tau = \tau_0 (p/p_0)^\alpha (r/r_2)^s$ in $r > r_2$.

Harder momentum spectra are obtained as ϵ increases. For $\epsilon = 0$, one obtains the free-escape boundary spectral index obtained by Webb et al. (2019; Rieger & Duffy 2019 obtain a similar result for μ_∞ by using a leaky box model). In the limit as $\epsilon \to \infty$, the spectral index $\mu_\infty \to 3 + \alpha$, which is the spectral index for shear acceleration obtained by Berezhko (1982) and Rieger & Duffy (2006) for the case of space independent solutions of the particle transport equation due to shear acceleration (these authors noted that $f_0 \propto p^{-(3+\alpha)}$ as $t \to \infty$ in their time-dependent Green's function solution at sufficiently large p). The curves of μ_∞ versus β_0 in Figure 3 converge to the asymptote $\mu_\infty = 3 + \alpha$ for relativistic jets as $\beta_0 \to 1$. Harder spectra are obtained as ϵ increases, verifying the idea that shear flows with adjacent regions in which the particles can scatter back into the shear flow are better for particle acceleration. However, one should also keep in mind that if the particles originate at large distances from the jet (i.e., at $r \gg r_2$), then these particles will be impeded from entering the shear flow region $0 < r < r_2$ if there is strong scattering (small $\tau(r, p)$) in $r > r_2$. Strong shear gradients of the flow inside $0 < r < r_2$ also lead to effective particle acceleration.

In Section 5, an overall discussion is given of viscous shear acceleration in radio jets. Section 5.1 presents a generalized telegrapher equation for cosmic-rays derived by Webb et al. (2018b). The equation is an extension of the diffusive cosmic-ray transport equation of Webb (1989), including the effects of cosmic-ray inertia. The diffusive telegrapher equation for a near isotropic distribution function was not derived here (because of length) but will be addressed in a separate paper. Section 5.2 gives a calculation of the mean time $\langle t(p; p_0)\rangle$ for particles to be accelerated from $p = p_0$ to momentum p, based on the time-dependent Green's function for shear acceleration obtained by Berezhko (1982) and by Rieger & Duffy (2006). For $p > p_0$, we find for reasonable values of α ($\tau \propto (p/p_0)^\alpha$) that $p\, d\langle t(p; p_0)\rangle/dp \sim p/\langle \Delta p/\Delta t\rangle$, where $\langle \Delta p/\Delta t\rangle$ is the systematic momentum drift term in the momentum diffusion transport equation. Section 5.3 discusses the use of leaky box models of particle acceleration similar to Rieger & Duffy (2019) and Webb et al. (2019) including viscous shear acceleration, synchrotron losses, and particle escape. The model is used to discuss the steady-state power-law index μ_∞ of shear accelerated particles (Sections 3 and 4) and how it is modified by synchrotron losses and particle escape. Section 5.4 discusses timescale estimates for the particle transport and acceleration and losses and the role of these processes in determining μ_∞.

Liu et al. (2017), Webb et al. (2019), and Rieger & Duffy (2019) give constraints on the acceleration of UHECR (e.g., $E = 10^{18}$ eV protons), in extragalactic radio jets by the viscous shear acceleration in extragalactic radio sources. The constraints are as follows: (i) the width of the jet ΔL needs to be greater than the mean free path λ and the particle gyroradius; (ii) the particle acceleration time $t_{\rm acc}$ needs to be less than the synchrotron loss time $t_{\rm synch}$; and (iii) $t_{\rm acc}$ needs to be less than the dynamical advection time $t_{\rm dyn}$ along the jet axis, limiting the possible values of the magnetic field strength B and jet width ΔL for particles with energy E in relativistic jets by the cosmic-ray viscosity acceleration mechanism. For example, it was found that to obtain protons with $E = 10^{18}$ eV $= 1$ EeV requires that ΔL must lie in the range 1 kpc $< \Delta L < 10^5$ kpc for the case where $B = 1\ \mu$G for a radio jet with a Lorentz factor $\gamma_j = 1.1$ (i.e., $\beta_0 = 0.4166$). It was suggested that the sources MKN501 and MKN421 (Dermer 2007; Sahayanathan 2009; Abbasi et al. 2014; Caprioli 2015) are possible sources of EeV protons accelerated by the cosmic-ray viscosity mechanism.

The telegrapher equation formula $p = p_{\max}(t) = p_0 \exp(\sqrt{\Gamma}\, t/\tilde{\gamma})$ for the maximum particle momentum, based on the telegrapher equation characteristics (i.e., (107)), implies a lower limit to the time required to accelerate particles in a jet shear flow. Taking $p_0 = 1\ {\rm GeV}\, c^{-1}$ and $\Delta L = 1$ kpc,

$p = p_{\max} = 1\ \mathrm{EeV}\ c^{-1}$ implies the particles are accelerated on a minimum timescale of 10^5–10^6 yr for a mildly relativistic jet, which is about 100 light-crossing times across the jet (Webb et al. 2019). Thus, the telegrapher equation characteristics and bi-characteristics can be useful in putting constraints on the acceleration time for particles initially with momentum $p = p_0$.

le Roux et al. (2019) use the nonrelativistic flow analog of Equation (100), (103), or (104) to model energetic particle acceleration in the solar wind due to contracting and reconnecting small-scale flux ropes in the vicinity of the Earth (their Equation (3)), which contains other transport and acceleration processes than those given by Equations (100) or (103). le Roux et al. (2019) refer to their transport equation as the telegrapher Parker transport equation, which is a modification of the diffusive transport equation for cosmic-rays obtained by, e.g., Parker (1965), Krymsky (1964), Gleeson & Axford (1967), Dolginov & Toptygin (1966, 1967), Jokipii & Parker (1970), and Skilling (1975). le Roux et al. (2019) show causality constraints on the particle transport and acceleration, which depend on the second-order derivatives and characteristics of their equation. Similar ideas on the constraints on the particle transport and acceleration by shear flow energization were also investigated by Webb et al. (2018a, 2018b, 2019), but further work on this problem is needed. However, this issue will not be investigated further here as it lies beyond the scope of the present investigation.

G.M.W. acknowledges discussions with Frank Rieger on particle acceleration by cosmic-ray viscosity in radio-jet shear flows. We thank the referee for pointing out numerical errors in Section 5.4 in formulae for τ_{re} for synchrotron cooling and for critical assessment of the manuscript. G.M.W. and G.L. were supported in part by NASA grant 80NSSC19K0075. J.A.le.R. is supported in part by NASA grants NNX15A165G, 80NSSC19K0276, and NSF-DOE grant PHY-1707247. G.P. Z. has been supported in part by the NSF EPSCoR RII-Track-1 Cooperative Agreement OIA-1655280 and an NSF/DOE Partnership in Basic Plasma Science and Engineering via NSF grant PHY-1707247. P.M. was supported in part by John Hopkins University Applied Physics Laboratory independent R&D funds. A.F.B. acknowledges valuable insights and discussions with Prof. Peter Biermann on UHECR and candidate sources and radio galaxies.

Appendix A

In this appendix section, we outline the derivation of the Green's function solution of Equation (46) using the Fourier–Bessel series approach described in Appendix A of Webb et al. (2019), Equation (144) et seq. We use the Fourier–Bessel solution ansatz of Equation (35).

To obtain the Green's function, we first write $\delta(\eta - \eta_1)$ in the form

$$\delta(\eta - \eta_1) = \sum_{n=1}^{\infty} c_n J_0(\lambda_n \eta), \tag{A1}$$

which is a Fourier–Bessel expansion for $\delta(\eta - \eta_1)$. By using Bessel's equation, we obtain the relations

$$(\lambda_m^2 - \lambda_n^2) \int_0^{\eta_2} \eta J_0(\lambda_m \eta) J_0(\lambda_n \eta) d\eta = [W_{mn}\eta]_0^{\eta_2}, \tag{A2}$$

where

$$W_{mn} = g_m(\eta)\frac{dg_n}{d\eta} - g_n(\eta)\frac{dg_m}{d\eta} \quad \text{and} \quad g_n(\eta) = J_0(\lambda_n \eta). \tag{A3}$$

Here, W_{mn} is the Wronskian of $g_m(\eta)$ and $g_n(\eta)$. Note that the eigenvalues $j_n = \lambda_n \eta_2$ satisfy the eigenvalue Equation (38), which depends crucially on the parameter $\epsilon = k/s$, and in general $\epsilon \neq 0$.

Using the eigenvalue Equation (38), we find

$$W_{mn}(\eta_2) = \frac{1}{\epsilon\eta_2}[g_n(\eta_2)g_m(\eta_2) - g_m(\eta_2)g_n(\eta_2)] = 0. \tag{A4}$$

Similarly, $\lim_{\eta\to 0}[\eta W_{mn}(\eta)] = 0$. Thus, Equation (A2) implies the orthogonality relations

$$\int_0^{\eta_2} \eta g_m(\eta) g_n(\eta)\, d\eta = N_n \delta_{mn}, \tag{A5}$$

where

$$N_n = \lim_{\lambda_m \to \lambda_n} \frac{1}{\lambda_m^2 - \lambda_n^2}[\eta W_{mn}]_0^{\eta_2}. \tag{A6}$$

Using the eigenvalue Equation (38) to evaluate N_n in Equation (A6), we obtain

$$\begin{aligned} N_n &= \frac{1}{2}\eta_2^2[J_0'(j_n)^2 + J_0(j_n)^2] \\ &\equiv \frac{1}{2}\eta_2^2[J_0(j_n)^2 + J_1(j_n)^2] \\ &\equiv \frac{1}{2}\eta_2^2 J_1(j_n)^2(1 + \epsilon^2 j_n^2). \end{aligned} \tag{A7}$$

The case where $r = r_2$ is a free-escape boundary was treated by Webb et al. (2019). It corresponds to the limit $\epsilon \to 0$ in Equations (38) and (A7).

To determine the c_n coefficients in the delta function expansion of Equation (A1), pre-multiply Equation (A1) by $\eta J_0(\lambda_m \eta)$ and integrate over η from $\eta = 0$ to $\eta = \eta_2$ and use the orthogonality relations in Equation (A5) to obtain

$$c_n = \eta_1 J_0(\lambda_n \eta_1)/N_n, \tag{A8}$$

for the constants $\{c_n\}$ in Equation (A1). Next, substitute the eigenfunction expansion in Equation (A1) into the transport Equation (28) and use the representation of Equation (A1) for $\delta(\eta - \eta_1)$ in the source term in Equation (28). Equating the $J_0(\lambda_n \eta)$ terms equal to zero in the equation gives the ordinary differential equation

$$\frac{d^2 h_n}{dT^2} + 2a\frac{dh_n}{dT} - 5\lambda_n^2 h_n(T) = -5A c_n \delta(T). \tag{A9}$$

Here, the source term in Equation (28) is written in the form $-A\delta(T)\delta(\eta - \eta_1)$ where

$$A = \frac{3N_0}{8\pi^2 p_0^3 c^2 \tau_0 k \eta_1}. \tag{A10}$$

The homogeneous Equation (A9) has independent solutions

$$y_1 = \exp[-(a + \chi_n)T], \quad y_2 = \exp[(\chi_n - a)T] \tag{A11}$$

where

$$\chi_n = \sqrt{a^2 + 5\lambda_n^2}. \tag{A12}$$

The Wronskian of y_1 and y_2 is given by

$$W(y_1, y_2) = y_1 y_2' - y_2 y_1' = 2\chi_n \exp(-2aT). \tag{A13}$$

The general solution of the inhomogeneous ordinary differential Equation (A9) is given by the general formula

$$h_n(T) = y_1\left(c_1 - \int^T \frac{Q(T')y_2(T')}{W_{T'}(y_1, y_2)}\,dT'\right) + y_2\left(c_2 + \int^T \frac{Q(T')y_1(T')}{W_{T'}(y_1, y_2)}\,dT'\right), \tag{A14}$$

(Morse & Feschbach (1953), Vol. 1, p. 530, 5.2.19), where $W_T(y_1, y_2) = y_1 dy_2/dT - y_2 dy_1/dT$ is the Wronskian of the two independent solutions y_1 and y_2 of the homogeneous Equation (A9), which are listed in Equation (A11). Q is the source term in Equation (A9). Using Equation (A14) to solve the inhomogeneous Equation (A9) and requiring $h_n(T)$ to be bounded as $T \to \pm\infty$, we obtain the required solution of Equation (A9) in the form

$$h_n(T) = \frac{5Ac_n}{2\chi_n}\exp[-aT - \chi_n|T|). \tag{A15}$$

Using A from Equation (A10) and using Equations (A7) and (A8) to obtain c_n gives $h_n(T)$ in Equation (A15). Using these results in Equation (35) gives the Green's function solution in Equation (46).

Appendix B

In this appendix section, we note that for a separable diffusion coefficient of the form

$$\kappa(r, p) = \kappa_1(r)\kappa_2(p), \tag{B1}$$

the boundary condition of Equation (14) at $r = r_2$ reduces to

$$f_0(r_2, p) + \left(r_2\kappa_1(r_2)\int_{r_2}^{\infty} \frac{dr'}{r'\kappa_1(r')}\right)\left(\frac{\partial f_0(r, p)}{\partial r}\right)_{r_2} = f_0(\infty, p). \tag{B2}$$

More simply, this boundary condition can be written as

$$\left[f_0(r, p) + r\frac{\partial f_0}{\partial r}\Phi(r_2)\right]_{r_2} = f_0(\infty, p), \tag{B3}$$

where

$$\Phi(r_2) = \int_{r_2}^{\infty} \frac{dr'\kappa_1(r_2)}{r'\kappa_1(r')}. \tag{B4}$$

For the case $\kappa_1(r) = (r/r_2)^s$, we obtain

$$\Phi(r_2) = \int_{r_2}^{\infty} \frac{dr'}{r'}\left(\frac{r'}{r_2}\right)^{-s} = \frac{1}{s}, \tag{B5}$$

which reproduces the boundary condition of Equation (17) in this case.

Appendix C

In this appendix section, we derive the formula (119) for the mean time $\langle t(p)\rangle$ for particles to be accelerated from momentum $p = p_0$ up to (or down to) momentum p due to particle acceleration by cosmic-ray viscosity in shear flows, based on the Green's function of Berezhko (1982), i.e., Equation (114). To evaluate $\langle t(p)\rangle$ requires that we determine the two integrals given below

$$K_0 = \int_0^{\infty} f_0(p, t)\,dt, \quad K_1 = \int_0^{\infty} tf_0(p, t)\,dt, \tag{C1}$$

and their ratio

$$\langle t(p)\rangle = \frac{K_1}{K_0}, \tag{C2}$$

where $f_0(p, t)$ is the Green's function of Berezhko (1982), i.e., Equation (114).

We first note that the Green's function in Equation (114) can be expressed in the form

$$f_0 = \frac{A(p)}{t}\exp\left(-\frac{\lambda_1}{t}\right)I_\nu\left(\frac{\lambda_2}{t}\right), \tag{C3}$$

where

$$A(p) = \frac{Q_0}{\alpha\Gamma\tau_0 p_0}(\bar{p})^{-a}, \quad a = \frac{3+\alpha}{2},$$
$$\lambda_1 = \frac{1 + (\bar{p})^{-\alpha}}{\alpha^2\Gamma\tau_0}, \quad \lambda_2 = \frac{2}{\alpha^2\Gamma\tau_0}(\bar{p})^{-\alpha/2}. \tag{C4}$$

Using the change of integration variable $\tilde{t} = 1/t$, the integrals K_0 and K_1 reduce to

$$K_0 = A(p)\int_0^{\infty} d\tilde{t}\,\exp(-\lambda_1\tilde{t})\frac{1}{\tilde{t}}I_\nu(\lambda_2\tilde{t}),$$
$$K_1 = A(p)\int_0^{\infty} d\tilde{t}\,\exp(-\lambda_1\tilde{t})\frac{1}{\tilde{t}^2}I_\nu(\lambda_2\tilde{t}). \tag{C5}$$

Notice that K_0 and K_1 are Laplace transforms with respect to λ_1.

Using the Laplace transform

$$\int_0^{\infty} \exp(-st)\left[\frac{1}{t}I_\nu(\alpha t)\right]dt = \frac{1}{\nu}\alpha^\nu[s + (s^2 - \alpha^2)^{1/2}]^{-\nu}, \tag{C6}$$

($\mathrm{Re}(s) > |\mathrm{Re}(\alpha)|$ with $s \to \lambda_1$ and $\alpha \to \lambda_2$: Erdelyi et al. 1954, Vol. 1, formula 4, p. 195), we obtain

$$K_0 = A_0(\bar{p})^{-a}[(\bar{p})^{-2a}H(p - p_0) + (\bar{p})^{2a}H(p_0 - p)], \tag{C7}$$

where

$$A_0 = \frac{Q_0}{\alpha\Gamma\tau_0 p_0}. \tag{C8}$$

Similarly, K_1 can be evaluated by using the Laplace transform

$$\int_0^{\infty} dt\,\exp(-st)[t^\mu I_\nu(\alpha t)] = \Gamma(\mu + \nu + 1) \times [(s^2 - \alpha^2)^{1/2}]^{-\mu-1}P_\mu^{-\nu}\left(\frac{(s^2 - \alpha^2)^{1/2}}{s}\right), \tag{C9}$$

(Erdelyi et al. 1954, Vol. 1, p. 196, formula 8, where $\mathrm{Re}(\mu+\nu) > -1$, $\mathrm{Re}(s) > |\mathrm{Re}(\alpha)|$). Using the transform of Equation (C9) with $s \to \lambda_1$, $\alpha \to \lambda_2$, $\mu = -2$ in Equation (C5), we obtain

$$K_1 = A_0(\bar{p})^{-a}\Gamma(\nu-1)\frac{|1-(\bar{p})^{-\alpha}|}{\alpha^2\Gamma\tau_0}P_{-2}^{-\nu} \times \left(\frac{|1-(\bar{p})^{-\alpha}|}{\alpha^2\Gamma\tau_0}\frac{\alpha^2\Gamma\tau_0}{1+(\bar{p})^{-\alpha}}\right). \tag{C10}$$

Equation (C6) is equivalent to Equation (116), and Equation (C10) is equivalent to Equation (118). The formula in Equation (119) for $\langle t(p)\rangle$ follows from Equation (C2). Note that the existence of K_1 requires $0 < \alpha < 3$ (we assume that $\alpha > 0$, but Jokipii et al. (1989) studied the case where the mean free path $\lambda \propto p^{-2}$).

The moment

$$K_n = \int_0^\infty t^n f_0(p, t)\, dt, \tag{C11}$$

can also be calculated using the transform of Equation (C9), provided that $0 < \alpha < 3/n$. In that case, we obtain

$$K_n = A_0(\bar{p})^{-a}\Gamma(\nu-n)\left(\frac{|1-(\bar{p})^{-\alpha}|}{\alpha^2\Gamma\tau_0}\right)^n P_{-(n+1)}^{-\nu} \times \left(\frac{|1-(\bar{p})^{-\alpha}|}{\alpha^2\Gamma\tau_0}\frac{\alpha^2\Gamma\tau_0}{1+(\bar{p})^{-\alpha}}\right). \tag{C12}$$

The condition $0 < \alpha < 3/n$ implies that for a fixed α, $n < 3/\alpha$.

A more standard approach to calculating the moments is to introduce the Laplace transform of $f_0(p, t)$ as

$$\bar{f}_0(s, p) = \int_0^\infty \exp(-st) f_0(p, t)\, dt. \tag{C13}$$

Then, note that

$$\frac{d\bar{f}_0(s, p)}{ds} = -\int_0^\infty t\exp(-st) f_0(p, t)\, dt,$$
$$\frac{d\bar{f}_0(s, p)}{ds}\Big|_{s=0} = -\int_0^\infty t f_0(p, t)\, dt. \tag{C14}$$

Also note that

$$\bar{f}_0(0, p) = \int_0^\infty f_0(p, t)\, dt. \tag{C15}$$

From Equation (C14), we obtain

$$\langle t(p)\rangle = \frac{\int_0^\infty t f_0(p, t)\, dt}{\int_0^\infty f_0(p, t)\, dt} = -\left(\frac{d\bar{f}_0/ds}{\bar{f}_0(s, p)}\right)_{s=0}. \tag{C16}$$

Similarly,

$$\langle t^n(p)\rangle = (-1)^n\left(\frac{d^n\bar{f}_0/ds^n}{\bar{f}_0(s, p)}\right)_{s=0}. \tag{C17}$$

In the present application,

$$\bar{f}_0(s, p) = \int_0^\infty \exp(-st)\frac{A_0\bar{p}^{-a}}{t}\exp\left(\frac{\lambda_1}{t}\right) I_\nu\left(\frac{\lambda_2}{t}\right) dt. \tag{C18}$$

The Laplace transform $\bar{f}(s, p)$ in Equation (C18) may be evaluated by using the transform

$$\int_0^\infty \exp(-st)\left\{\frac{1}{t}\exp\left(-\frac{(\tilde{\alpha}+\tilde{\beta})}{2t}\right) I_\nu\left(\frac{(\tilde{\alpha}-\tilde{\beta})}{2t}\right)\right\} dt = 2K_\nu[(\sqrt{\tilde{\alpha}}+\sqrt{\tilde{\beta}})\sqrt{s}]\, I_\nu \times [(\sqrt{\tilde{\alpha}}-\sqrt{\tilde{\beta}})\sqrt{s}] \tag{C19}$$

(Erdelyi et al. 1954, Vol. 1, p. 200, formula 4: $\mathrm{Re}(s) > 0$, $\mathrm{Re}(\tilde{\alpha}) > \mathrm{Re}(\tilde{\beta}) > 0$). To evaluate Equation (C18), we set

$$\lambda_1 = \frac{\tilde{\alpha}+\tilde{\beta}}{2}, \quad \lambda_2 = \frac{\tilde{\alpha}-\tilde{\beta}}{2},$$
$$\tilde{\alpha} = \lambda_1 + \lambda_2, \quad \tilde{\beta} = \lambda_1 - \lambda_2, \tag{C20}$$

which allows us to determine $\bar{f}_0(s, p)$ and its derivatives at $s = 0$, which in turn leads to expressions for the moments $\langle t^n(p)\rangle$ by using Equation (C17).

From Equation (C20), we obtain

$$\tilde{\alpha} = \frac{(1+(\bar{p})^{-\alpha/2})^2}{\alpha^2\Gamma\tau_0}, \quad \tilde{\beta} = \frac{(1-(\bar{p})^{-\alpha/2})^2}{\alpha^2\Gamma\tau_0}. \tag{C21}$$

Using Equations (C19) and (C21) in Equation (C18) gives

$$\bar{f}_0(s, p) = 2A_0(\bar{p})^{-a} \times \{K_\nu(\chi\sqrt{s}) I_\nu(\chi(\bar{p})^{-\alpha/2}\sqrt{s}) H(\bar{p}-1) + K_\nu(\chi(\bar{p})^{-\alpha/2}\sqrt{s}) I_\nu(\chi\sqrt{s}) H(1-\bar{p})\}, \tag{C22}$$

where

$$\chi = \frac{2}{\alpha\sqrt{\Gamma\tau_0}}. \tag{C23}$$

The general moment $\langle t^n(p)\rangle$ can now be determined by using Equation (C22) in Equation (C17).

ORCID iDs

G. M. Webb https://orcid.org/0000-0002-0617-9502
P. Mostafavi https://orcid.org/0000-0002-3808-3580
G. Li https://orcid.org/0000-0003-4695-8866
J. A. le Roux https://orcid.org/0000-0001-9199-2890
G. P. Zank https://orcid.org/0000-0002-4642-6192

References

Abbasi, R. U., Abe, M., Abu-Zayyad, T., et al. 2014, ApJL, 790, L21
Abramowitz, M., & Stegun, I. A. 1965, Handbook of Mathematical Functions (New York: Dover)
Achterberg, A. 1979, A&A, 76, 276
Achterberg, A., Gallant, Y. A., Kirk, J. G., & Guthman, A. W. 2001, MNRAS, 328, 393
Achterberg, A., & Norman, C. A. 2018a, MNRAS, 479, 1747
Achterberg, A., & Norman, C. A. 2018b, MNRAS, 479, 1771
Araudo, A. T., Bell, A. R., Blundell, K. M., & Mathews, J. H. 2018, MNRAS, 473, 3500
Araudo, A. T., Bell, A. R., Crilly, A., & Blundell, K. M. 2016, MNRAS, 460, 3554
Axford, W. I. 1981, ICRC (Paris), 12, 155
Axford, W. I. 1994, ApJS, 90, 937
Axford, W. I., Leer, E., & Skadron, G. 1977, ICRC (Plovdiv), 11, 132
Drury, L. O'C., Axford, W. I., & Summers, D. 1982, MNRAS, 198, 833
Bell, A. R. 1978a, MNRAS, 182, 147

Bell, A. R. 1978b, MNRAS, 182, 443
Bell, A. R., Mathews, J. H., Blundell, K. M., & Araudo, A. T. 2019, MNRAS, 487, 4571
Berezhko, E. G. 1981, ICRC (Paris), 3, 506
Berezhko, E. G. 1982, SvAL, 8, 403
Berezhko, E. G. 1983, ICRC (Bangalore), 2, 279
Berezhko, E. G., & Krymsky, G. F. 1981, SvAL, 7, 352
Bicknell, G. V., & Melrose, D. B. 1982, ApJ, 262, 511
Biermann, P. L., & Strittmatter, P. A. 1987, ApJ, 322, 643
Blandford, R. D., & Ostriker, J. P. 1978, ApJL, 221, L29
Blandford, R. D., Simeon, P., & Yuan, Y. 2014, NUPhS, 256, 9
Caprioli, D. 2015, ApJL, 811, L38
Dermer, C. D. 2007, ICRC (Merida, Yucatan), 6, 95
Dolginov, A. Z., & Toptygin, I. N. 1966, Izv. Akad. Nauk SSSR Ser. Fiz, 30, 1780
Dolginov, A. Z., & Toptygin, I. N. 1967, Ge&Ae, 7, 785
Drake, J. F., Swisdak, M., & Fermo, R. 2013, ApJL, 763, L5
Drury, L. O'C. 1983, RPPh, 46, 973
Earl, J. A., Jokipii, J. R., & Morfill, G. E. 1988, ApJL, 331, L91
Erdelyi, A., Magnus, W., Oberhettinger, F., & Tricomi, F. G. 1954, Tables of Integral Transforms (New York: McGraw-Hill)
Gleeson, L. J., & Axford, W. I. 1967, ApJL, 149, L115
Guo, F., Liu, Y.-H., Daughton, W., & Li, H. 2015, ApJ, 806, 167
Hillas, A. M. 1984, ARA&A, 22, 425
Jokipii, J. R., Kota, J., & Morfill, G. E. 1989, ApJL, 345, L67
Jokipii, J. R., & Morfill, G. E. 1990, ApJ, 356, 255
Jokipii, J. R., & Parker, E. N. 1970, ApJ, 160, 735
Khabarova, O. V., Zank, G. P., Malandraki, O. E., le Roux, J. A., & Webb, G. M. 2017, SunGe, 12, 23
Kimura, S. S., Kohta, M., & Zhang, B. T. 2018, PhRvD, 97, 023026
Kirk, J. G., & Duffy, P. 1999, JPhG, 25, R163
Kirk, J. G., & Schneider, P. 1987a, ApJ, 315, 425
Kirk, J. G., & Schneider, P. 1987b, ApJ, 322, 256
Krülls, W. 1992, A&A, 260, 49
Krymsky, G. F. 1964, Ge&Ae, 4, 763
Krymsky, G. F. 1977, DoSSR, 234, 1306
le Roux, J. A., Webb, G. M., Khabarova, O. V., Zhao, L. L., & Adhikari, L. 2019, ApJ, 887, 77
le Roux, J. A., Zank, G. P., Webb, G. M., & Khabarova, O. 2015, ApJ, 801, 112
le Roux, J. A., Zank, G. P., Webb, G. M., & Khabarova, O. 2016, ApJ, 827, 47
Lemoine, M. 2019, PhRvD, 99, 083006
Li, X., Guo, F., Li, H., & Li, G. 2017, ApJ, 843, 21
Liu, R. 2015, PhD thesis, Ruperto-Carola Univ., Heidelberg
Liu, R.-Y., Rieger, F. M., & Aharonian, F. A. 2017, ApJ, 842, 39
Malkov, M., & Drury, L. O'C. 2001, RPPh, 64, 429
Matthews, J. H., Bell, A. R., Blundell, K. M., & Aurodo, A. T. 2019, MNRAS, 482, 4303
Morse, P. M., & Feschbach, H. 1953, Methods of Theoretical Physics, Vol. 1 (New York: McGraw-Hill)
Ohira, Y. 2013, ApJL, 767, L16
Ostrowski, M. 1990, A&A, 238, 435
Ostrowski, M. 1998, A&A, 335, 134
Ostrowski, M. 2002, MNRAS, 312, 579
Parker, E. N. 1965, P&SS, 13, 9
Pelletier, G., Bykov, A., Ellison, D., & LeMoine, M. 2017, SSRv, 207, 319
Protheroe, R. J., & Szabo, A. P. 1992, PhRvL, 69, 2885
Rachen, J. P., & Biermann, P. L. 1993, A&A, 272, 161
Rachen, J. P., Stanev, T., & Biermann, P. L. 1993, A&A, 273, 377
Rieger, F. M. 2019, Galax, 7, 78
Rieger, F. M., & Duffy, P. 2004, ApJ, 617, 155
Rieger, F. M., & Duffy, P. 2005a, in AIP Conf. Proc. 801, Astrophysical Sources of High Energy Particles and Radiation, ed. P. Chen (Melville, NY: AIP), 365
Rieger, F. M., & Duffy, P. 2005b, in AIP Conf. Proc. 745, 2nd Int. Symp. on High Energy Gamma-Ray Astronomy, ed. F. A. Aharonian, H. J. Voelk, & D. Horns (Melville, NY: AIP), 745
Rieger, F. M., & Duffy, P. 2006, ApJ, 652, 1044
Rieger, F. M., & Duffy, P. 2016, ApJ, 833, 34
Rieger, F. M., & Duffy, P. 2019, ApJL, 886, L26
Rieger, F. M., & Mannheim, K. 2002, A&A, 396, 833
Sahayanathan, S. 2009, MNRAS, 398, L49
Schlickeiser, R. 2002, Cosmic Ray Astrophysics (Berlin: Springer)
Skilling, J. A. 1975, MNRAS, 172, 557
Sneddon, I. N. 1957, Elements of Partial Differential Equations, International Student edition (New York: McGraw-Hill)
Stawarz, L., & Ostrowski, M. 2002, ApJ, 578, 763
Webb, G. M. 1983, ApJ, 270, 319
Webb, G. M. 1985, ApJ, 296, 319
Webb, G. M. 1989, ApJ, 340, 1112
Webb, G. M. 1990, ICRC (Adelaide), 4, 126
Webb, G. M., Al-Nussirat, S., Mostafavi, P., et al. 2019, ApJ, 881, 123
Webb, G. M., Barghouty, A. F., Hu, Q., & le Roux, J. A. 2018a, ApJ, 855, 31
Webb, G. M., Barghouty, A. F., leRoux, J. A., et al. 2018b, AGUFM, SH11D-2908
Webb, G. M., Drury, L. O'C., & Biermann, P. 1984, A&A, 137, 185
Webb, G. M., Jokipii, J. R., & Morfill, G. E. 1994, ApJ, 424, 158
Webb, G. M. 1987, ApJ, 321, 606, Erratum for Relativistic Transport Theory for Cosmic Rays (Webb, G. M., 1985, ApJ, 296, 319)
Zank, G. P., Hunana, P., le Roux, J. A., et al. 2015, ApJ, 814, 137
Zank, G. P., le Roux, J. A., Webb, G. M., Dosch, A., & Khabarova, O. 2014, ApJ, 797, 28